Master's Thesis
석사 학위논문

in-vivo Blood Flow Detection using Diffuse Speckle Contrast Analysis

Chaebeom Yeo（여 채 범 呂 彩 汎）

Department of Robotics Engineering

로봇공학전공

DGIST

2016

Master's Thesis
석사 학위논문

in-vivo Blood Flow Detection using Diffuse Speckle Contrast Analysis

Chaebeom Yeo（여 채 범 呂 彩 汎）

Department of Robotics Engineering

로봇공학전공

DGIST

2016

in-vivo Blood Flow Detection using Diffuse Speckle Contrast Analysis

Advisor : Professor Cheol Song

Co-advisor : Professor Kijoon Lee

By

Chaebeom Yeo
Department of Robotics Engineering
DGIST

A thesis submitted to the faculty of DGIST in partial fulfillment of the requirements for the degree of Master of Science in the Department of Robotics Engineering. The study was conducted in accordance with Code of Research Ethics[1]

1. 8. 2016

Approved by

Professor Cheol Song (Advisor) (Signature)

Professor Kijoon Lee (Co-Advisor) (Signature)

[1] Declaration of Ethical Conduct in Research**:** I, as a graduate student of DGIST, hereby declare that I have not committed any acts that may damage the credibility of my research. These include, but are not limited to: falsification, thesis written by someone else, distortion of research findings or plagiarism. I affirm that my thesis contains honest conclusions based on my own careful research under the guidance of my thesis advisor.

in-vivo Blood Flow Detection using Diffuse Speckle Contrast Analysis

Chaebeom Yeo

Accepted in partial fulfillment of the requirements
for the degree of Master of Science.

11. 24. 2015

Head of Committee	Prof. Cheol Song	(인)
Committee Member	Prof. Kijoon Lee	(인)
Committee Member	Prof. Heejaung Kim	(인)

MS/RT
201423004

여 채 범. Chaebeom Yeo. *in-vivo* Blood Flow Detection using Diffuse Speckle Contrast Analysis. Department of Robotics Engineering. 2016. 42p. Advisors Prof. Cheol Song, Co-Advisors Prof. Kijoon Lee.

ABSTRACT

Stable circulation is essential for healthy life. In contrast, circulatory disturbance could cause cardiovascular diseases such as stroke and cardiac death. Recently, statistical data showed that 25 % of cause of death in Korea is related to circulatory system. The blood flow detection in early stage is essential for prevention of the cardiovascular disease. To diagnose these kinds of diseases which is originated from circulatory disturbance, blood flow measurement system requires frequent inspection, non-invasive measurement, and high data acquisition speed. Previous studies on blood flow measurement such as implantable arterial blood flow sensor and ultrasound imaging have been reported. However, these inspection methods are invasive or inefficient. Here, we suggest diffuse speckle contrast analysis (DSCA) system which performs non-invasive estimation for the blood flow, which is dependent on the correlation of speckle pattern caused by the blood flow. DSCA system could offer simple data analysis, flexibility, and fast measurement speed compared to previous studies. Since the DSCA system could achieve 1 Hz data acquisition rate and deep blood flow measurement, *in-vivo* experiments are available in human skin, chick embryo, erectile dysfunction, and ischemic stroke rat brain. Results show the validation of the DSCA system by various experiments with phantom, human skin, chick embryo, erectile dysfunction, and rat brain. In the phantom experiment, the DSCA system shows almost linear correlation between the blood flow index and the induced Intralipid flow. In the chick embryo experiment, comparative experiment between healthy embryo and weakened embryo prove that DSCA system could detect a vital sign of embryo. The blood flow index of healthy embryo is much higher than weakened embryo. The stroke rat brain experiment shows that infarct area has less blood flow index than contralateral area. Erectile dysfunction and human arm experiments indicate the effectiveness of the measurement system by

measuring real-time change of blood flow index caused by stimulation or pressure, respectively. With various data analyses and configurations, the performance of DSCA system was evaluated on various samples and proved effectiveness of the DSCA system for blood flow measurement. From this study, the DSCA system could secure *in-vivo* measurement of blood flow in deep tissues. In future work, the DSCA system will be useful in medical diagnostic device.

Keywords: Blood flow, Diffuse speckle contrast analysis, BFI, Speckle, Micro-circulation

Contents

List of Figures

List of Tables

1. Introduction

1.1 Study Background

Stable blood circulation plays an important role in preserving the physical health because blood flow transports nutrients, preserves body temperature, and maintains cell-level metabolism [1,2]. It is related to blood pressure, among other vital signs used to assess basic body functions. Lack of blood flow could be lead to a variety of diseases such as ischemic stroke, peripheral artery disease (PAD), and carotid artery disease (CAD). Those are critical disease in USA, as shown in fig. 1. Therefore, fast and accurate blood flow measurement system for diagnosis of the various diseases are required.

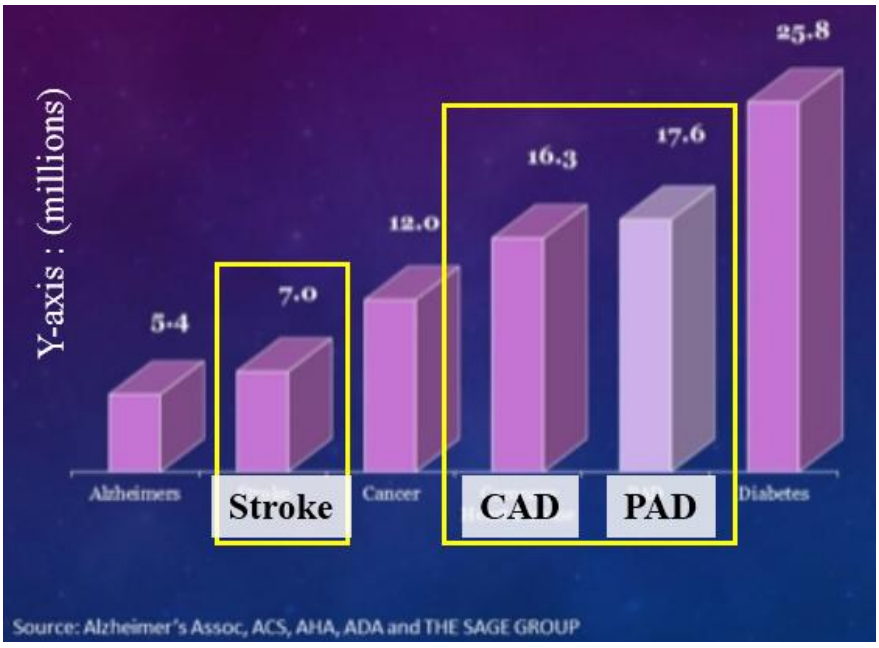

Figure 1. Prevalence of major disease in USA (in 2010).

1.2 Previous Studies

Existing methods for blood flow measurement in clinical experiments include computational tomography (CT) angiography, magnetic resonance imaging (MRI) based arterial spin labeling (ASL-MRI), laser doppler flowmetry (LDF), laser speckle contrast analysis (LSCA), diffuse correlation spectroscopy (DCS), and optical coherence tomography (OCT) angiography, etc. Although CT and ASL-MRI give 3D imaging with high resolution, the limitations are high cost, low imaging acquisition speed, and radiographic exposure. In case of the LDF, LSCA, and OCT, it is mostly used on superficial layer because those have low measuring depth. The DCS could measure deep blood flow, relatively. However, it requires complicate hardware setup and signal processing.

Several imaging studies in biology have been developed to measure blood flow in the hearts of chick embryos using particle image velocimetry (PIV) [3], photoacoustic tomography (PAT), and OCT [4,5]. These invasive techniques are practically limited in poultry farming. However, various non-invasive techniques used to measure the fertility of avian embryos have been proposed. Candling is frequently used on poultry farms due to the simple and fast measurement [6]. Inspectors monitor the daily volume change of blood vessels and the movement of an embryo by illuminating the egg with a bulb in a dark room. However, vital signs after early incubation stages of incubation could not be precisely and quantitatively measured because of the high absorption of light. Micro-MRI has been used to establish 3D images of chick embryos, but it is not practically useful solution for poultry farms in aspect of low image acquisition speed and the high cost [7]. Laser speckle imaging (LSI) systems have been applied to image the vasculature of chick embryo in the early incubation stage [8]. The LSI system visualizes a blood flow map from speckle intensity fluctuations caused by embryonic vasculatures under laser illumination and could distinguish embryonic fertilization.

However, this system does not detect the development of embryos after six days of incubation. Another study using speckle phenomenon has analyzed heart rate of avian embryos from 13 to 19 days of incubation [9]. However, this system requires complicated hardware implementation, highly sensitive detectors, and it does not detect the vital sign in the early incubation stages. The Buddy digital egg monitor has measured heart rates of embryo after six days of incubation [10].

1.3 Study Purpose

Recently, diffuse speckle contrast analysis (DSCA) has been validated as a novel deep tissue flowmetry system with the advantages of a low cost, easy analysis, fast image acquisition time, and a simple experimental setup [11,12]. The instrumentation used in a DSCA system resembles that of diffuse correlation spectroscopy (DCS) [13–15], and data analysis is simple and similar to a LSI system [16–18]. DCS is a powerful tool for deep blood flow measurements; however, it requires complicated data processing and a highly sensitive photon detector. LSI can be used for full-field imaging of superficial layers. DSCA is capable of assessing deep tissue flow, based on the configuration of the DCS and simple data analysis of the LSI. Here, the objective of this study is to design and implement the DSCA system. As well as, it is to apply the DSCA into various biomedical fields. Although Lenzhe et al. has reported the DSCA system on the phantom and human arm [11,12], we present experimental results of phantom, human arm, chick embryo, erectile dysfunction, and stroke rat brain.

2. Diffuse Speckle Contrast Analysis (DSCA)

2.1 Theory

The DSCA system estimates the flow rate based on the correlation of the speckle intensity. When a long coherent laser fiber is illuminated and movement of scatters within a sample leads to reduction of the diffused speckle contrast for the given exposure time of CCD camera, as shown in Fig. 2. The high contrast on the region of interest (ROI) of CCD camera can be distinguished as slow blood flow inside the biological sample. On the other hands, the low contrast can be defined as the fast flow.

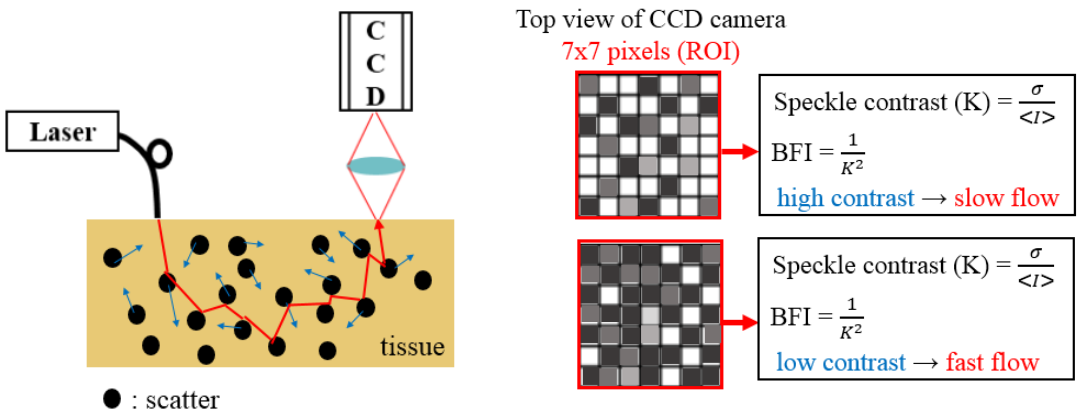

Figure 2. Principle of DSCA system.

Speckle contrast (K) in the data processing of the LSI system is computed as a ratio between standard deviation and average of speckle intensity at image pixels with same dimension, as described in Eq. (1) [19-22].

$$K = \frac{\sigma}{< I >} \tag{1}$$

The speckle contrast is derived by normalized electric field autocorrelation $g_1(\tau)$ at the given exposure time T of the CCD camera, as in following expression,

$$K^2(T) = V_N(T) = \frac{2p}{T}\int_0^T (1-\frac{\tau}{T})[g_1(\tau)]^2 d\tau \quad (2)$$

where V_N represents the normalized variance, τ is delay time, and p is constant dependent on the ratio of CCD chip size to speckle size.

Blood flow index (BFI) in DCS system is determined from unnormalized electric field autocorrelation $G_1(\tau)$, as shown in Eq. (3),

$$G_1(r,\tau) = \frac{3\mu'}{4\pi}\left[\frac{\exp(-h_D(\tau)r_1)}{r_1} - \frac{\exp(-h_D(\tau)r_2)}{r_2}\right]. \quad (3)$$

where $h_D(\tau) = \sqrt{3\mu_s'\mu_a + \alpha\mu_s'^2 h_0^2 < r^2(\tau) >}$, μ_s' , μ_a , α are the reduced scattering coefficient, absorption coefficient, the fraction of dynamic photon scattering events in medium, respectively. $r_1 = \sqrt{r^2 + z_0^2}$, $r_2 = \sqrt{r^2 + (z_0 + 2z_b)^2}$. r is a distance between the source and the detector. $z_0 = 1/\mu_s'$. $z_b = 2(1-R_{eff})/3\mu_s'(1+R_{eff})$, where R_{eff} is effective reflection coefficient. $< r^2(\tau) >$ is mean square displacement of the moving scatter after the delay time τ . The BFI of DCS system is mostly defined as αD_b for Brownian motion model [23,24]. The D_b represents effective diffuse coefficient.

In the DSCA system, the BFI could be derived as the relationship between K in the LSI and αD_b for the DCS by combining the Eq. (2) and (3). The linear relationship between the

$1/K^2$ and the αD_b is demonstrated. It is demonstrated that $1/K^2$ and αD_b are in linear relationship in the physiological blood flow range. Therefore, the BFI in the DSCA is defined as follows, [13-15]

$$BFI = \frac{1}{K^2} \tag{4}$$

2.2 Data analysis

Method	**Spatial domain analysis ("sDSCA")**	**Temporal domain analysis ("tDSCA")**
Advantage	**High temporal resolution** (fast data acquisition speed)	**High spatial resolution** (high quality of data analysis)
Disadvantage	**Low spatial resolution** (low quality of data analysis)	**Low temporal resolution** (slow data acquisition speed)

Table 1. Advantage and disadvantage of two data analysis.

In the data analysis of DSCA system, there are spatial and temporal domain analysis, as shown in table 1. Figure 3 shows spatial domain image processing. The speckle contrast in spatial domain (K_s) is calculated from the correlation of neighboring pixels in an image. The spatial domain analysis offers improved temporal resolution; however, it has low spatial resolution.

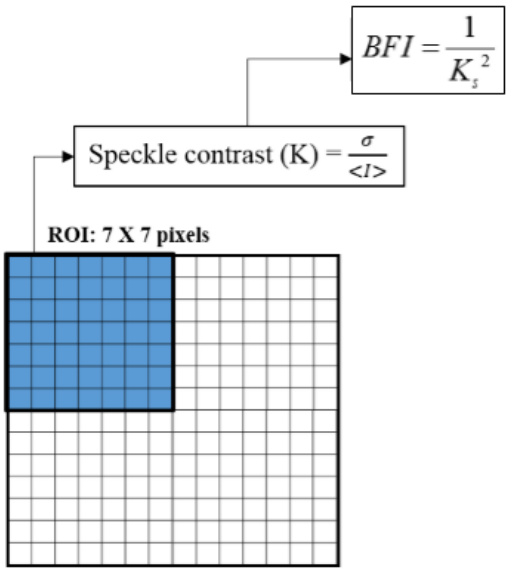

Figure 3. Schematic spatial domain analysis.

In the temporal domain, K_t is calculated by the correlation of pixels over time with same positions of specific images, as shown in fig. 4. The advantage of temporal domain analysis is high spatial resolution, however, it gives low temporal resolution.

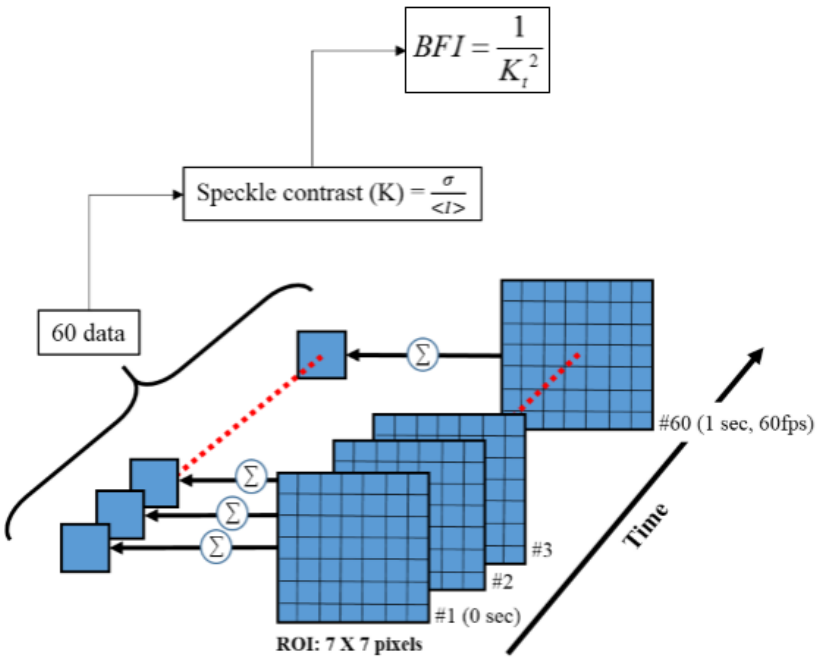

Figure 4. Schematic temporal domain analysis.

The relationship of two relationship is trade-off in the resolution. To acquire better spatial resolution, the temporal domain analysis in the data processing is used rather than the spatial domain in all experiments. However, two analysis methods are no significant difference. The exposure time and frame rate for the CCD camera were set to 50.027 ms and 20 fps, respectively. The speckle contrast computed from 20 images could produce a BFI data with a image acquisition rate of ~1 Hz. Each of data point is calculated from sum of elements of 7 by 7 pixel array as region of interest (ROI).

2.3 Configurations

Method	**Lens based DSCA**	**Fiber-optic based DSCA**
Advantage	**Simple measurement procedure**	**- Small motion artifact** **- Multi-channel measurement** (mDSCA)
Disadvantage	**Defocusing** (large motion artifact)	**Difficulty in fixing fibers to CCD chip**

Table 2. Advantage and disadvantage of two configurations.

In the experimental setup of DSCA system, there are lens based and fiber-optic based DSCA, as shown in table 2. Figure 5 shows configuration of the lens based DSCA. It offers simple measurement procedure; however, this method has defocusing problem caused by motion artifact.

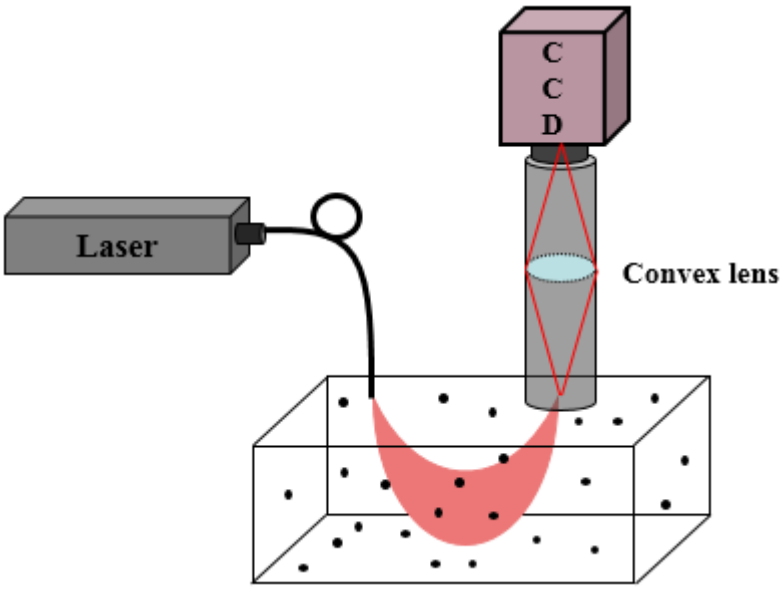

Figure 5. Lens based DSCA.

In the fiber-optic based DSCA, although it is difficult in connecting between optical fiber and charge coupled device (CCD) chip with close distance, this method reduce motion artifact by attaching on the sample, as shown in Fig. 6. Also, it could measure blood flow on various measurement positions, as shown in Fig. 7.

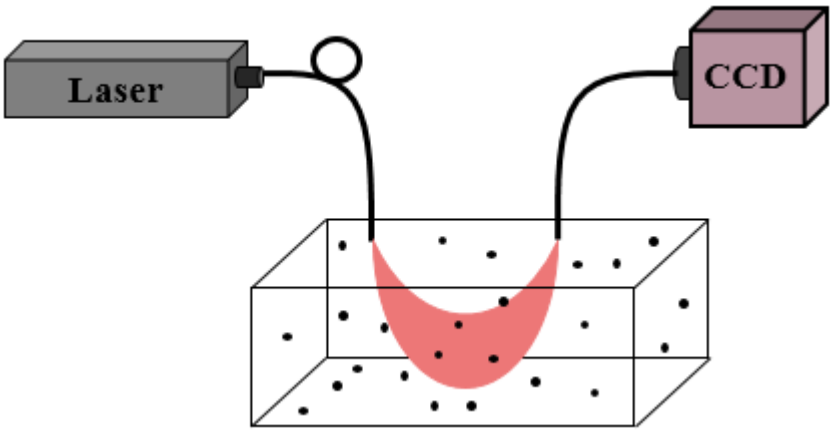

Figure 6. Fiber-optic based DSCA.

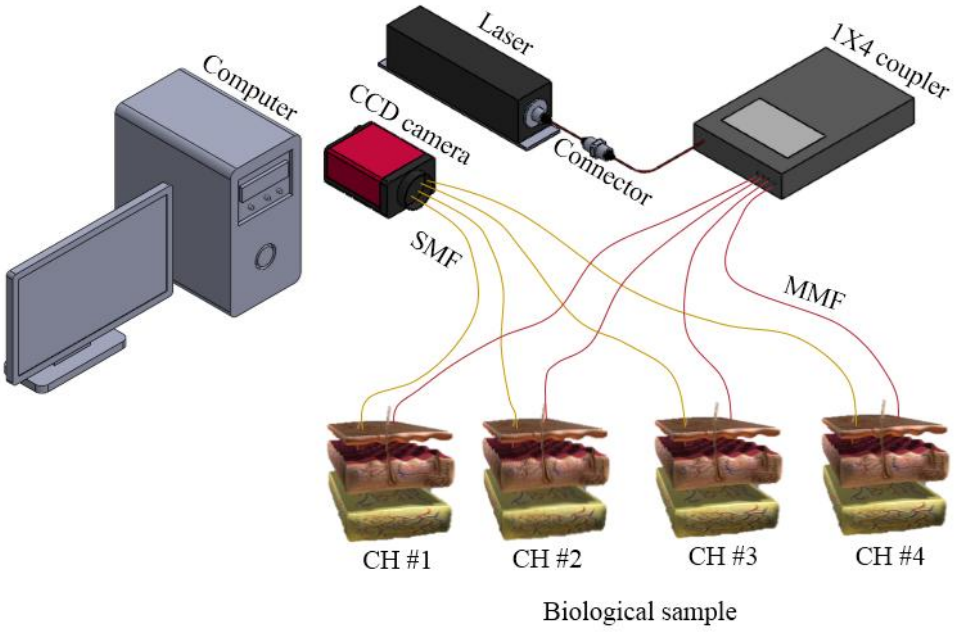

Figure 7. Configuration of multi-channel DSCA.

Figure 7 shows a schematic diagram of the multi-channel DSCA (mDSCA) in the fiber-optic based system for blood flow measurement inside biological samples. An optical fiber extended from a laser source (DL-785-100S, CrystaLaser, 785 nm, 100 mW) is coupled with a 1 × 4 coupler in order to separate the fiber into four multi-mode fibers (MMF).

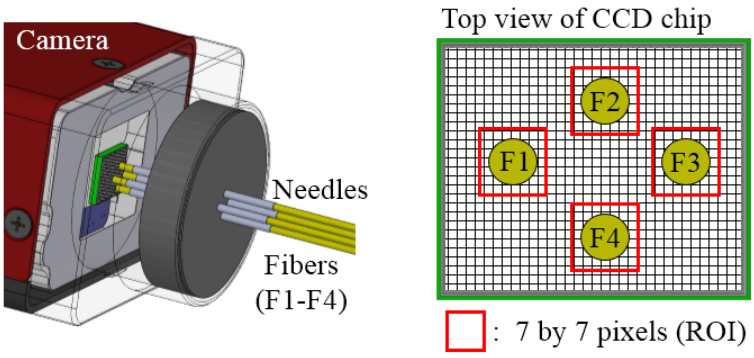

Figure 8. Detection channels.

A camera’s CCD detector chip (F-033B, Stingray, cell size: 9.9 um) is closely packed and fixed to four single-mode fibers (SMF, core size: 7 um) without physical contact, as shown in Fig. 8. The ROI of the CCD chip is accepted from 7 by 7 pixels, allowing the light intensity measured by each of detection fiber to be processed in its entirety. To avoid cross-talk, the distances between the four detection channels are maintained far enough. Instead of a photon detector, the CCD camera as detector is used to simplify the data processing and configuration of the detection channels. As well as, the advantages include simultaneous multi-channel detection and low cost.

3. Implementation of DSCA

3.1 Implementation

3.1.1 Lens based DSCA

Figure 9 shows the implementation of lens based DSCA system. Because the laser illumination with high power for long time could affect the biologically harmful effect, the laser is coupled with 1 by 4 coupler to reduce optical power (output power: 15 mW). The optical power is usually regulated up to 20 mW in biological sample when the laser illuminates for long time. The CCD camera is mounted with lens tube holder. The lens is 30 mm of focal length; the magnitude is set to one. Then, the CCD camera is connected with a computer. The inter-optode distance is set as 2.8 cm.

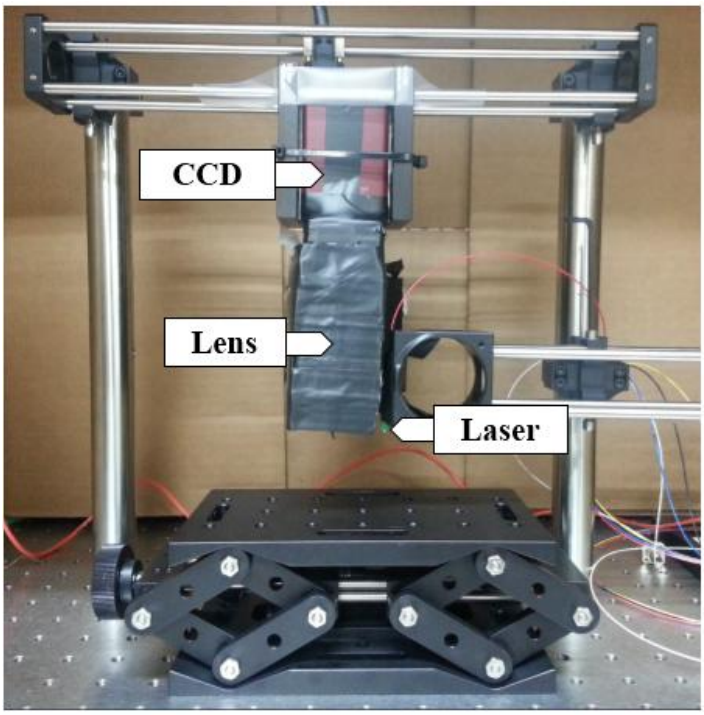

Figure 9. Implementation of lens based DSCA.

3.1.2 Fiber-optic based DSCA

Figure 10 displays the implementation of fiber-optic based DSCA system. The optical components are fixed on the aluminum plate of system box in order to prevent external force and vibration.

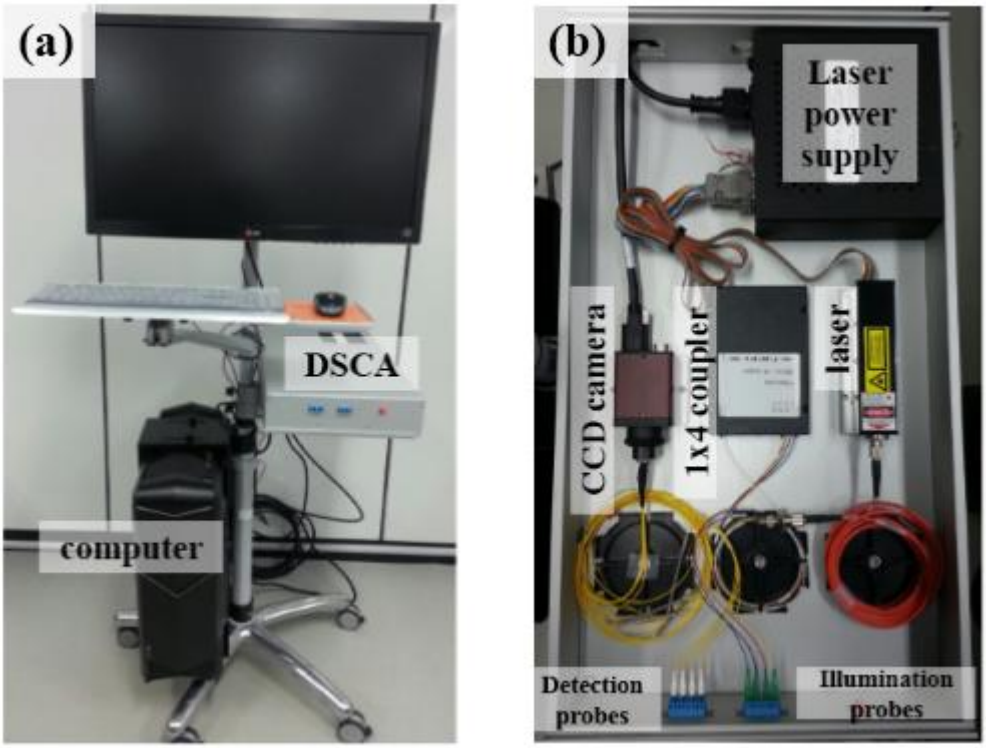

Figure 10. Implementation of fiber-optic based DSCA system. (a) Prototype of DSCA system. (b) Inner components of DSCA system box.

Figure 11 shows the end of measurement probes. Those are fixed with polydimethylsiloxane (PDMS) blocks; it is possible to vertically measure the BFI on the biological sample. On the other hands, Fig. 12 presents horizontal probes. The end of bared optical fibers are attached with aluminum foil to reflect vertically reflected protons. For more understanding, please refer Fig. 13 to 15.

Figure 11. End of multi-channel vertical probes.

(orange color fibers: laser, white color fibers: detector)

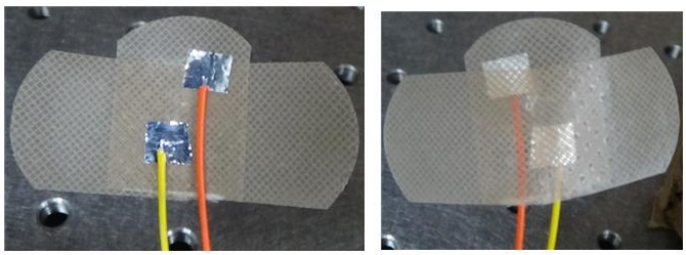

Figure 12. End of multi-channel horizontal probes.

(orange color fibers: laser, yellow color fibers: detector)

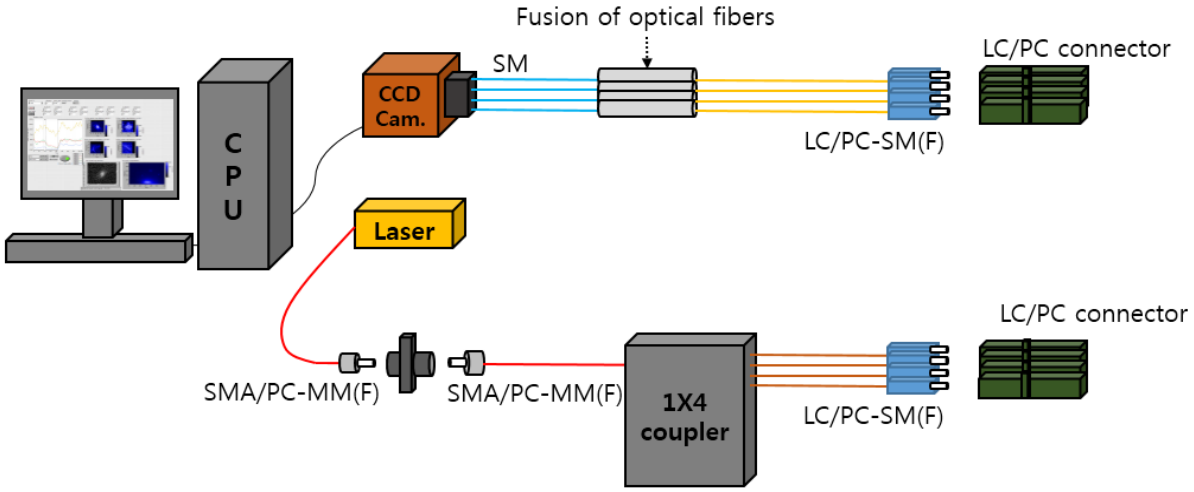

Figure 13. Schematic multi-channel DSCA in details.

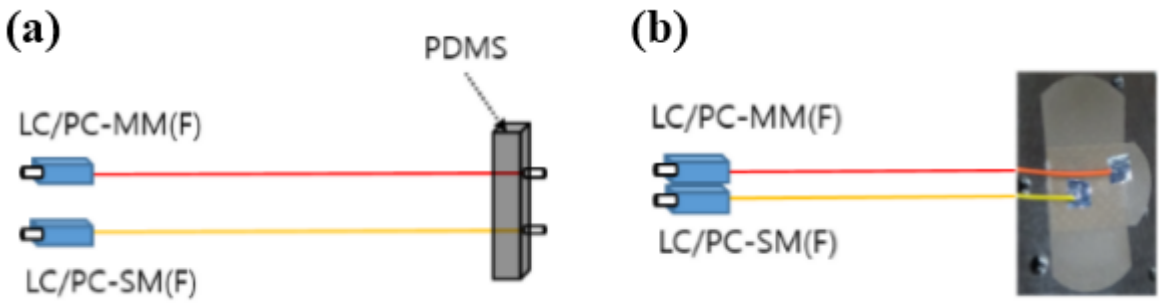

Figure 14. Schematic diagram of measurement probes. (a) vertical probe. (b) horizontal probe.

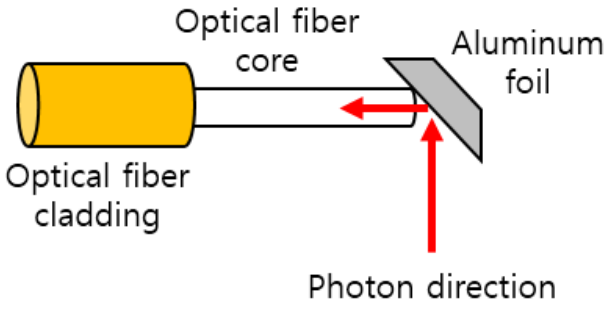

Figure 15. Schematic detection principle of horizontal probe.

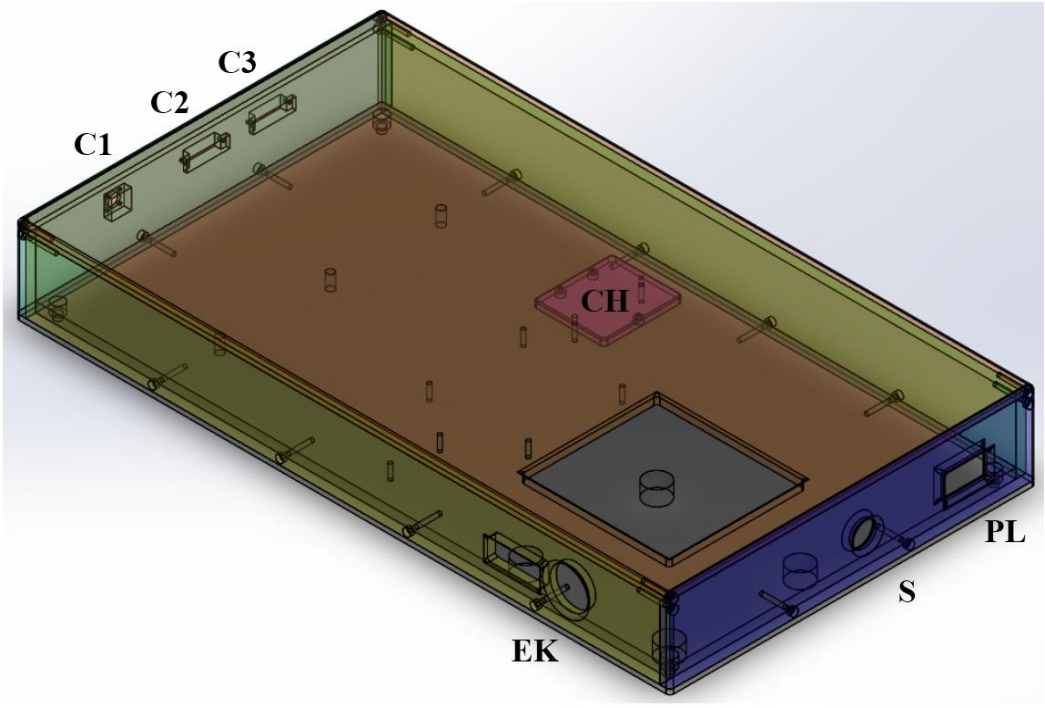

Figure 16. Cad design of DSCA box.

As shown in Fig. 10, the DSCA system is designed on the aluminum box in order to measure anywhere, conveniently. The aluminum box is designed as cad design (Solidworks Software), as shown in Fig. 16. C1, C2, and C3 are SMA patch cord connector holder, LC patch cord connector holder for illumination probes, and LC patch cord connector holder for detection probes. PL means the hole of laser power supply line and camera power line. S and EK are the hole of laser power supply switch, and the hole of laser power supply engine key, respectively. CH is the plate of CCD camera holder plate.

3.2 Performance evaluation

From the phantom study, we evaluated the lens based and fiber-optic based DSCA system. Figure 17 shows experimental setup on a phantom which is replaced to PDMS as biological sample. The flow velocity is changed from 0 to 24 ml/min in steps of 4 ml/min using syringe pump. The liquid as blood is used from Intralipid N 20%. The inter-optode distance is set as 28 mm.

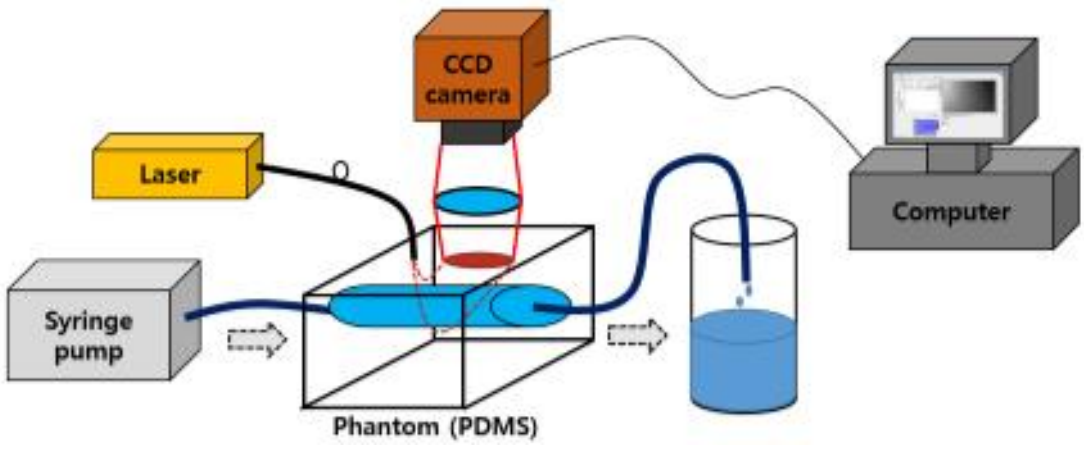

Figure 17. Experimental setup of lens based DSCA on phantom.

By increasing the flow velocity from a syringe pump, the BFI shows increasingly larger value, as shown in Fig. 18. At the each of step, the blue dots could not be shown significant differences. However, after the blue dots are averaged at the each of step, the difference are quietly distinct.

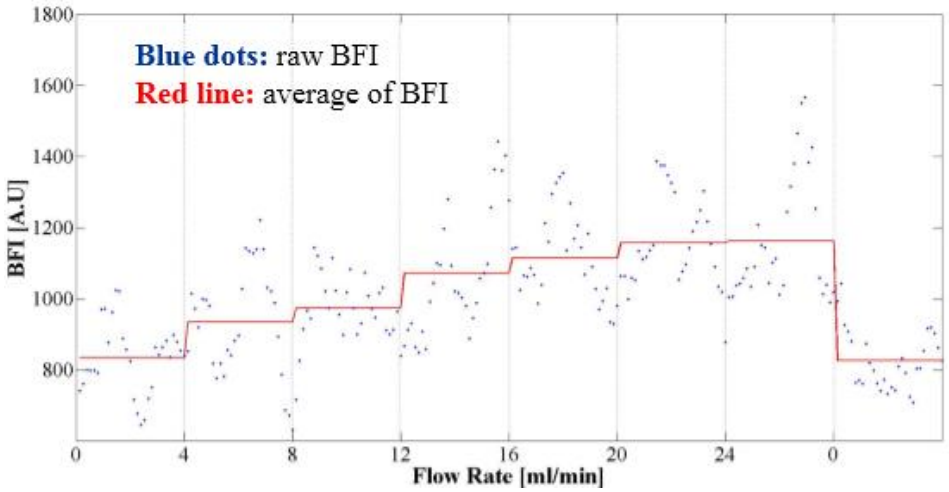

Figure 18. Experimental result of lens based DSCA on phantom.

Figure 19 and 20 displays experimental setup and result of fiber-optic based DSCA. In this experiment, the hole of phantom is densely filled up transparent beads with 3 mm of diameter in order to induce micro circulation. In the experimental protocol, the frame rate, exposure time, moving average are 60 fps, 15.726 ms, and 10, respectively. The result shows increase tendency by changing the flow velocity.

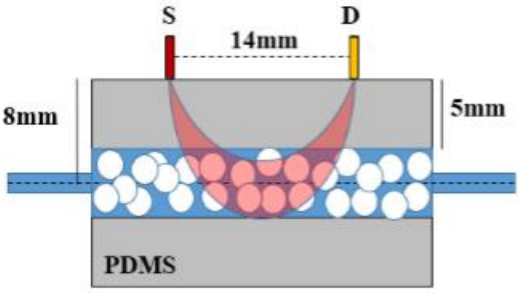

Figure 19. Experimental setup of fiber-optic based DSCA on phantom.

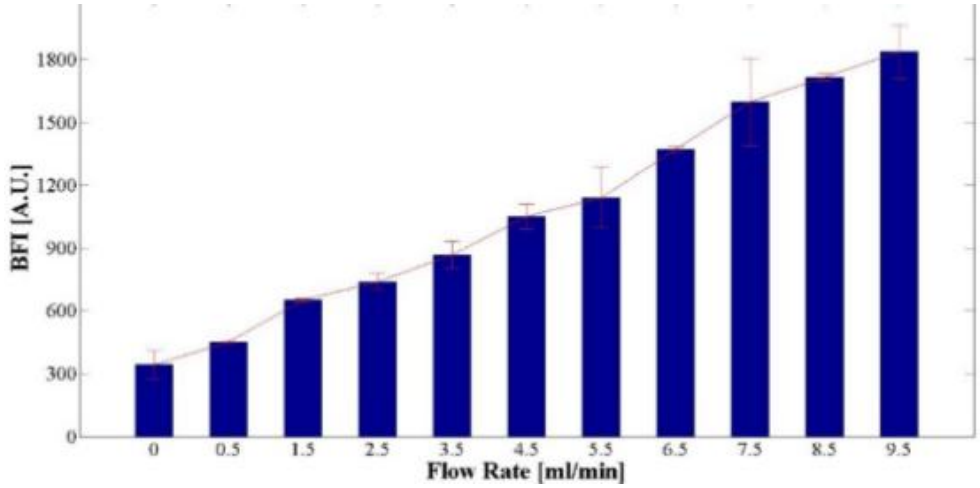

Figure 20. Experimental result of fiber-optic based DSCA on phantom.

Both results show linearity between BFI and flow rate. To compare sensitivity between lens based and fiber-optic based DSCA, the fiber-optic based system is larger than that of lens based system.

3.3 *in-vivo* applications

3.3.1 Human arm

To demonstrate DSCA performance in biological experiment, we applied on human arm. Figure 21 and 22 show experimental setup and result of lens based DSCA system on a human arm. The inter-optode distance is set as 28 mm. In experimental protocol, there are three periods: baseline, cuff-occlusion, and release periods. The period of baseline is formal blood flow state. The cuff-occlusion is the period that arm is blocked using blood pressure meter with 200 mmHg to induce blood flow occlusion. The period of release is that the pressure of the blood pressure meter is released. At the baseline for 70 sec, the BFI fluctuate around 1500 A.U. After this period, the BFI dramatically decreases at the cuff-occlusion period. And, the BFI significantly

increase after the cuff-occlusion period. Then, the BFI recover to baseline value after few minutes.

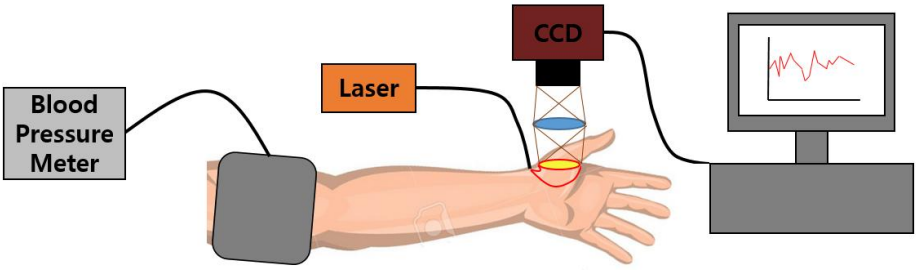

Figure 21. Experimental setup of lens based DSCA on human arm.

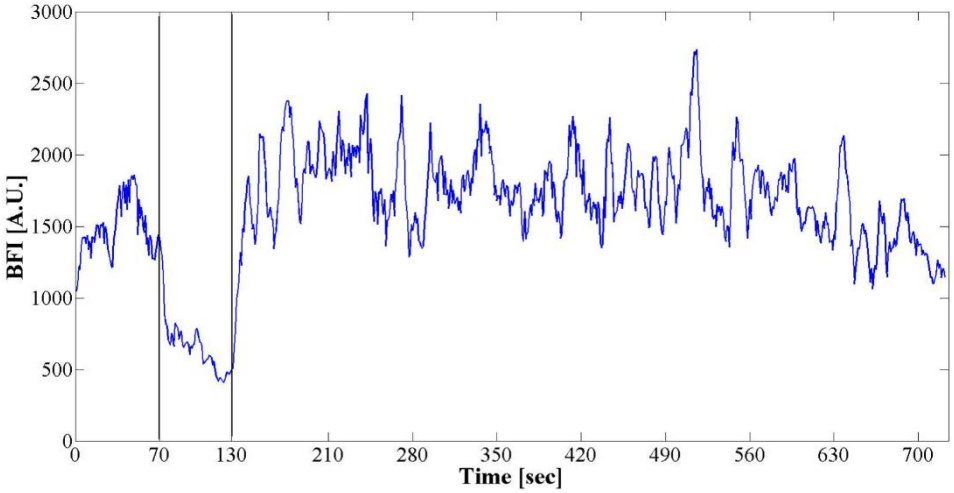

Figure 22. Experimental result of lens based DSCA on human arm.

As the Fig. 23, we attached multi-channel probes on human arm to analyze fiber-optic based DSCA system. Also, this experiment has three periods including baseline, cuff-occlusion, and release, controlled by a blood pressure meter. The inter-optode distance, frame rate, exposure time, moving average are 10 mm, 20 fps, 50.026 ms, and 15, respectively. At different periods, the BFI dramatically decreases and increases corresponding to the blood flow, as shown in Fig. 24. Interestingly, the BFIs show different magnitudes among measurement position at the release period. M4 is the position in which the volume of muscle is relatively

largest among measurement positions. Therefore, BFI of M4 shows relatively low change. M1 shows highest change, because the blood volume is best and muscle volume is least.

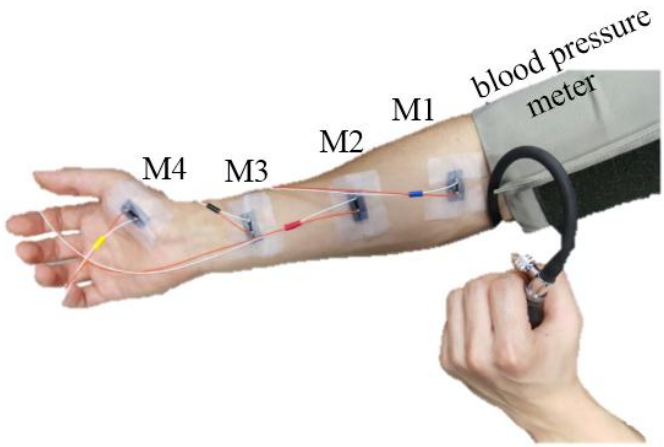

Figure 23. Experimental setup of fiber-optic based DSCA on human arm.

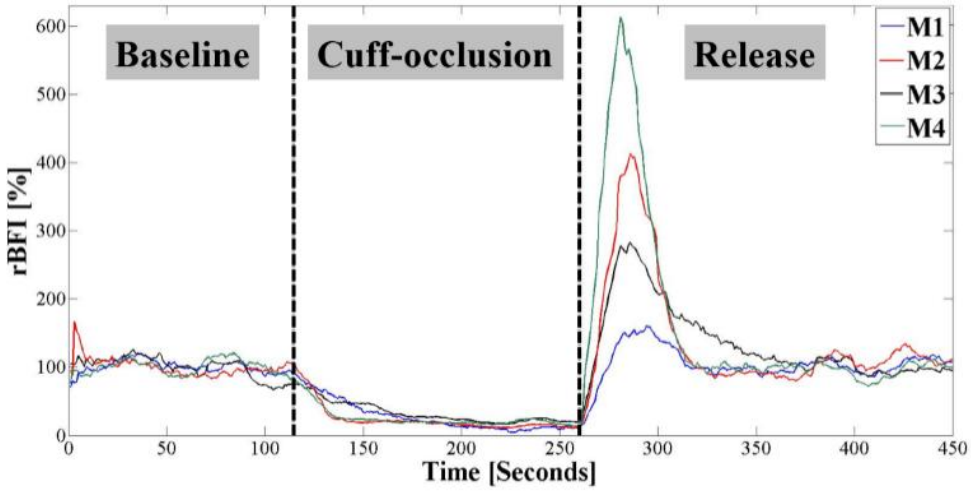

Figure 24. Experimental result of fiber-optic based DSCA on human arm.

Two experimental results show relative BFI (rBFI) changes corresponding to change of blood flow. In the sensitivity between two results, the fiber-optic based system is larger, because the change magnitude is higher than that of lens based system.

3.3.2 Chick embryo

Second *in-vivo* validation, we applied on chick embryo. Figure 25 show experimental setup of lens based DSCA and implantation of blood flow measurement of chick embryo.

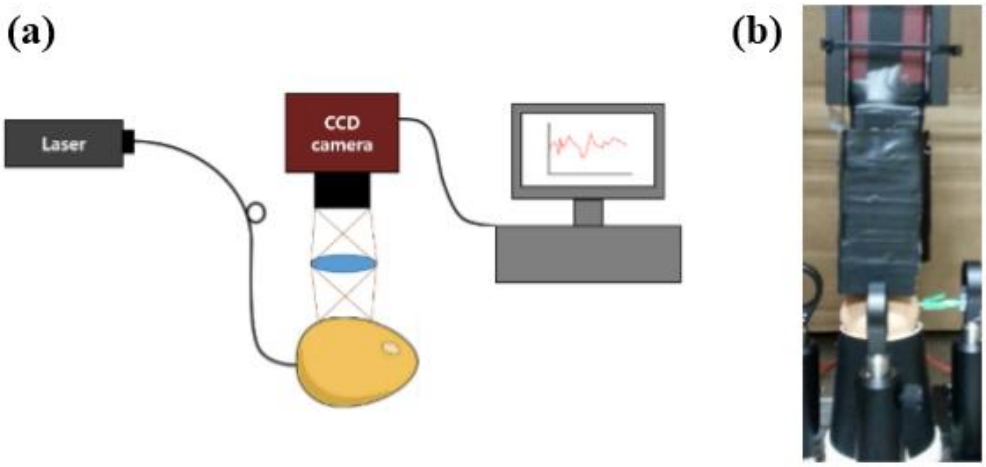

Figure 25. Experimental setup of lens based DSCA on chick embryo.

(a) Schematic diagram. (b) Implementation

Five eggs were incubated in an artificial incubator at 38 ± 0.1℃ and 75% humidity for 20 days, as shown in Fig. 26. The incubated egg group (N=5) is compared with non-incubated egg group (N=2). To induce a weakened embryo condition, three incubated eggs were cooled in a refrigerator at 5℃ for 300 min.

Figure 26. Artificial incubator.

In the experimental protocol, the laser illumination positions are set as four positions, as shown in Fig. 27. At the each of illumination position, measuring time is 200 sec, respectively. The inter-optode distance is set as 28 mm.

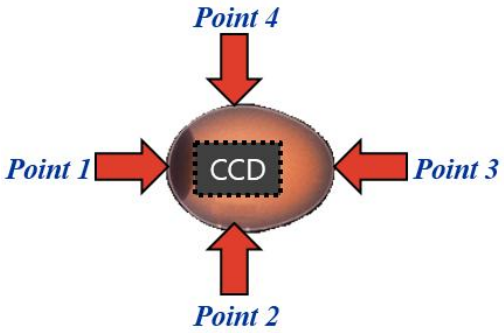

Figure 27. Four illumination positions.

Figure 28 shows BFI in the incubated egg on the 15th day of incubation at four illumination positions. Since every eggs have different organic structure and position at the each of point, the BFI has different value.

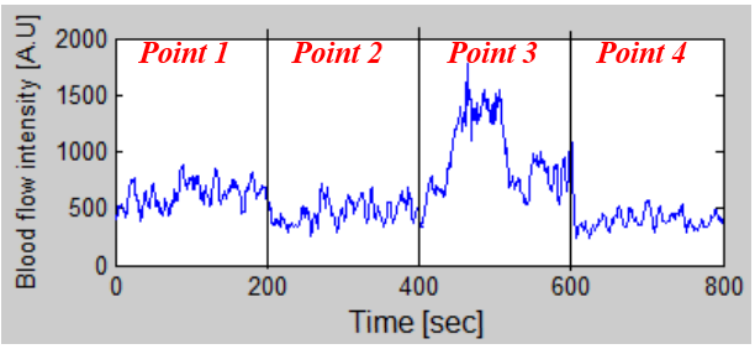

Figure 28. BFI of four illumination position in the incubated egg.

Figure 29 and 30 show comparison between incubated and non-incubated eggs. The color lines are incubated egg's BFI during 5 days. The black lines are non-incubated eggs. The BFIs

of incubated egg are larger than that of non-incubated eggs. When it applied with student's t-test, the difference can be clearly shown as 0.0114 of p-value ($p < 0.05$).

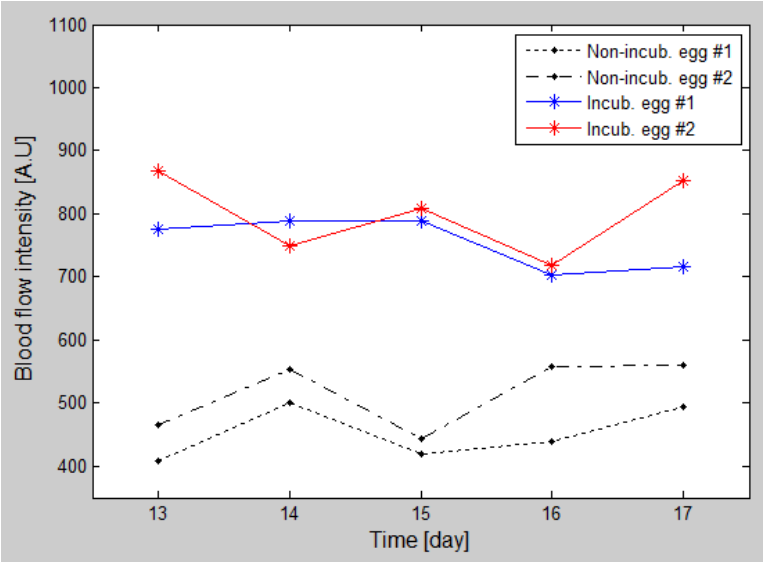

Figure 29. BFI changes of chick embryo from 13th day to 17th day of incubation.

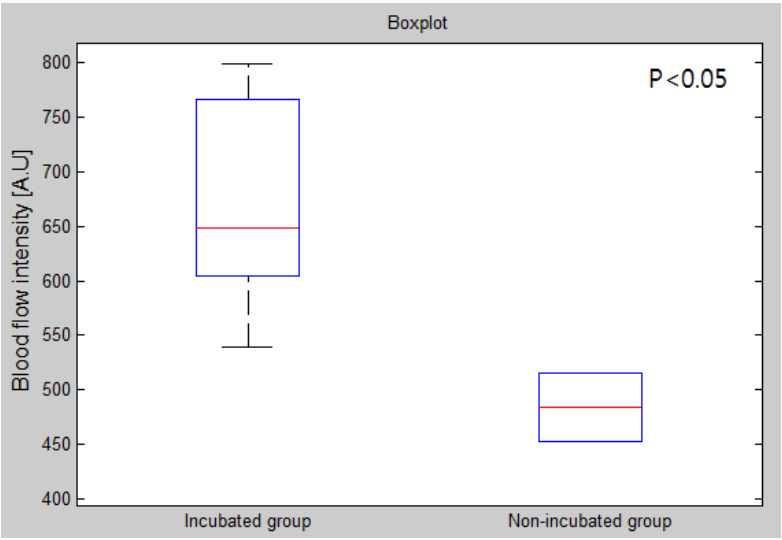

Figure 30. Boxplot of incubated and non-incubated egg groups.

Also, the comparison between live and weakened state in a same embryo shows significant difference at the illumination position 3, as shown in Fig. 31. Those results depict

that lens based DSCA system could detect vital sign of chick embryo. Although this experiment demonstrates DSCA performance for five days, we planning to analyze embryonic blood flow for whole incubation period with lens based DSCA in next time.

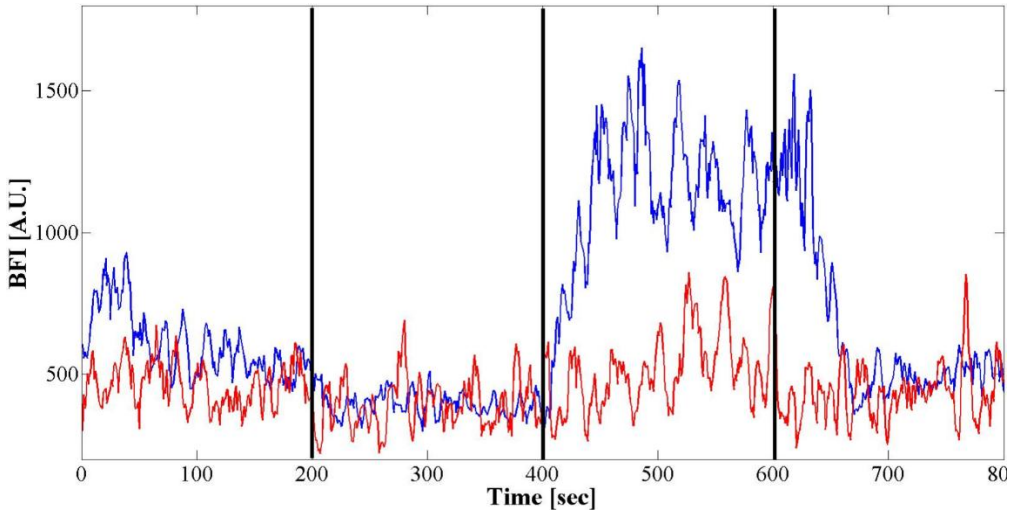

Figure 31. Comparison between live and weakened state in an embryo.

In the experiment of fiber-optic based DSCA system on the chick embryo, there are two kinds of studies. First experiment is the finding suitable inter-optode distance in the chick embryo experiment, as shown in Fig. 32.

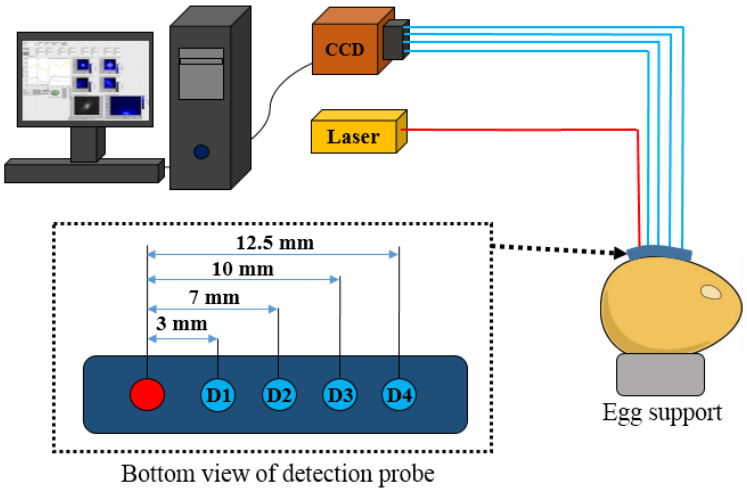

Figure 32. Scheme of chick embryo experiment using multiple depth detection probe.

The inter-optode distances (D1, D2, D3, and D4) are 3, 7, 10, and 12.5 mm, respectively. The more the inter-optode distance increases, the more the measuring depth in the eggshell increases. The flexible support of the detection probe is fabricated by PDMS; it could cover up the curvature of the eggshell. An egg is fixed on plastic ring as egg support for stable positioning.

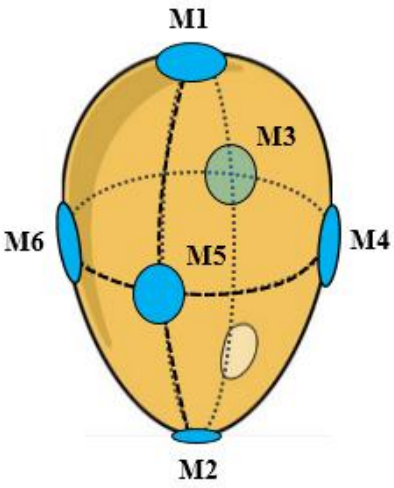

Figure 33. Scheme of six measurement position.

In the experimental protocol, the measurement positions from M1 to M6 are initially marked according to the organizational change of the chick embryo in the eggshell to analyze the overall blood flow in the eggshell, as shown in the Fig. 33. Each of the measurement position is examined for 100 seconds every day. Total data acquisition time is 10 minutes. The frame rate, exposure time, and moving average are 20 fps, 50.027, and 30, respectively.

In Fig. 34, to acquire the average of BFI change depending on the depth information, rBFI analysis at each of detection point (D1-D4) from average of six measurement positions (M1-M6) in the seven different eggs (N=7) are accomplished for 7 days of incubation. Day 0 represents the time before incubation. As the embryos gradually develop, most of the averages of the BFIs increase. During the early incubation stage, vasculature of embryo develops from

superficial layers of the egg shell, the BFIs in D1 and D2 are relatively high until 3 days. The BFI of D1 is relatively lower than the BFI of D2 and D3, because its measuring depth only reaches the egg shell. After 4 days, the BFIs of D3 and D4 are considerably higher than the others, because the blood vascular development is achieved in the deep depth. The change of BFI during early incubation period could be effectively distinguished on D1 and D2, whereas the change of BFI after the early incubation could be easily monitored on the D3 and D4.

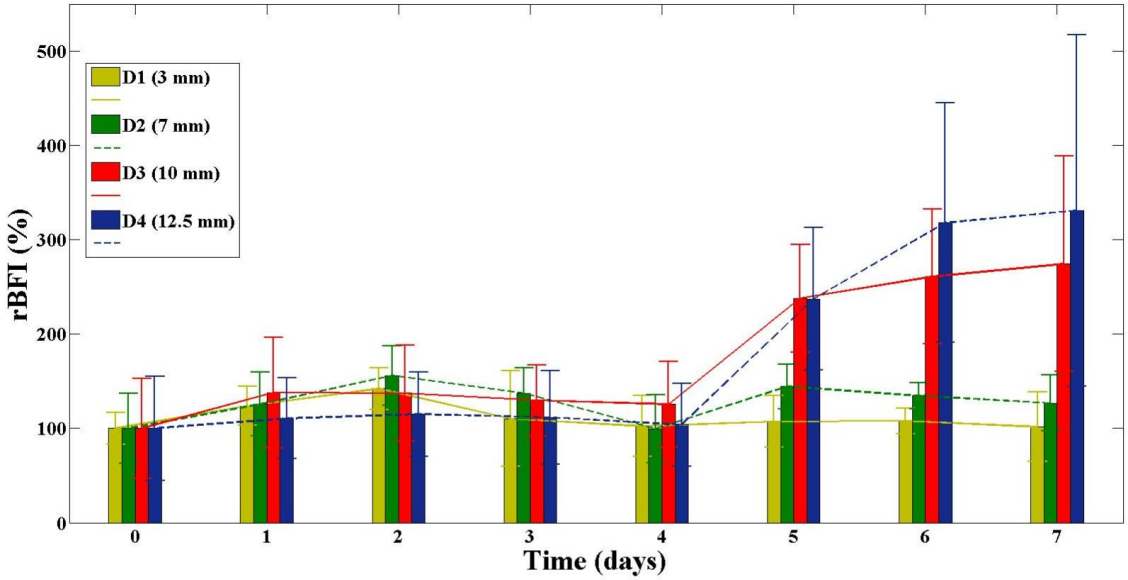

Figure 34. The mean BFI change depending on depth at four detection points.

Since D3 (detection point 3, 10 mm) shows the most distinct change of BFI from Day 1 to Day 7, we only employed data from D3 for the following analysis. Because each of the measurement position (M3, M4, M5, and M6) among seven eggs could not distinguish in early incubation stage, the mean of the BFI at these positions is calculated and shown in Fig. 35. The BFI of the M1 is relatively lower than other measurement positions due to the location of air cell. And, the BFI on the M2 with a few blood vessels and amount of albumen volume is relatively lower than the average from M3 to M6.

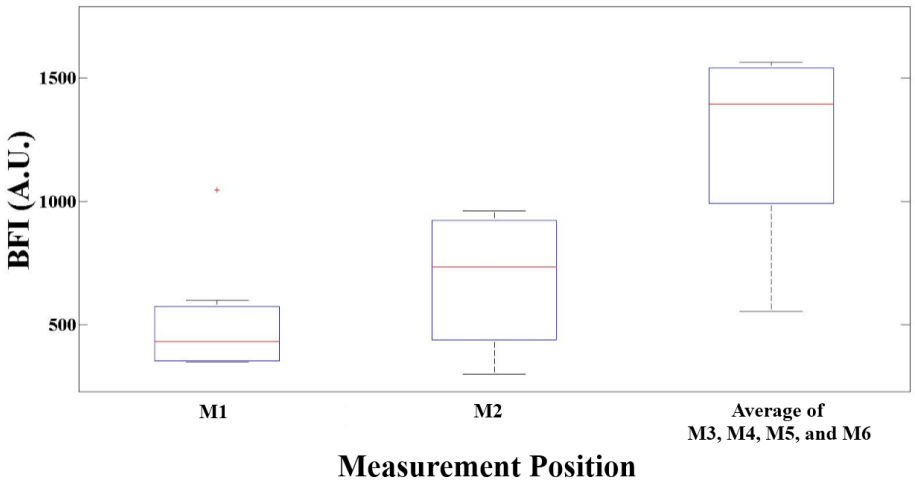

Figure 35. Boxplot from mean BFI of each measurement position on the detection point (D3)

Figure 36 shows the comparison between the BFIs of healthy and weakened states on average of all measurement points (M1-M6) at the detection point 3 (D3), which is achieved at the same eggs on Day 7 incubation. When student's t-test is applied, p-value achieved 0.0038 ($p < 0.05$). It represents that the BFIs between two groups have significant difference. Because the tissues of the weakened embryo does not have enough transportation of blood flow, its BFI is lower than the healthy embryo. This result shows that the DSCA system could determine whether the avian embryo survives in the early incubation period or not.

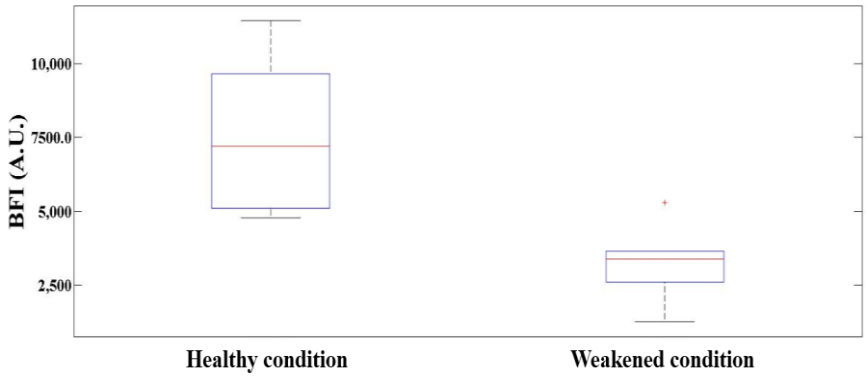

Figure 36. Comparison between the healthy and weakened embryos.

From previous chick embryo study, we find suitable inter-optode distance as 10 mm. In the second experiment of fiber-optic based DSCA system on the chick embryo, we experiment with this distance, as shown in Fig. 37 and 38. The egg support is designed to hold the egg and to allow contact with each detection probe through a small square hole. Four detection probes are located in flexible PDMS to change the inter-optode distance between the illumination and detection fibers.

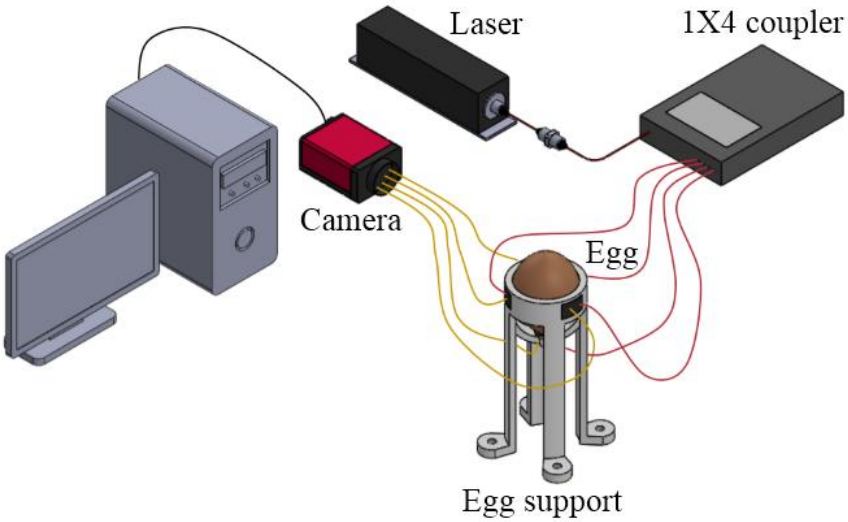

Figure 37. Schematic diagram of the mDSCA system.

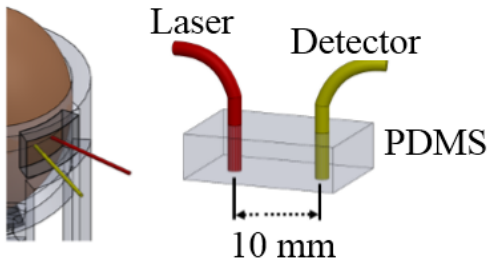

Figure 38. Scheme of a detection probe.

In the experimental protocol, the all measurement positions (M1–M4) were marked to measure the blood flow at the same positions, as shown in Fig. 39. Because the large end of

the egg has the air cell, measurement position is excluded. Total data acquisition time achieved for 200 seconds to gather a more accurate value for the 200 raw BFI over a 200 seconds period; the measurements were simultaneously performed on all positions. In this experiment, we used the term 'BFI' in order to represent the temporal average of raw BFIs for 200 seconds.

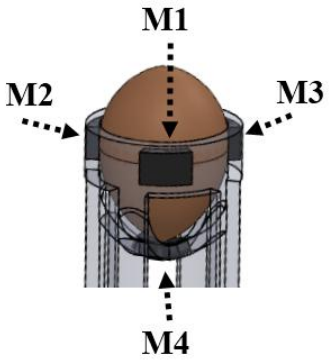

Figure 39. Four measurement positions of the egg support.

Figure 40 shows the relative change in the $< BFI >_S$ which represents the spatial average over all measurement positions. The error bar for each day means the discrepancy of BFIs among eleven eggs (N=11). The Day 0 is before the eggs are delivered into the artificial incubator. The $< BFI >_S$ increased because of embryonic development. It is similar to the study which measured mean heart rate of the chick embryo from Day 3 to Day 20 in the incubation period [9]. Even though the increase of heart rate might be correlated to the BFI increase [19], the BFI change during incubation period is mostly due to the increase of the number of blood vessels leading to the increase of blood volume. In the first quarter of the incubation period, the $< BFI >_S$ is relatively low, since the embryo heart and blood vessels become beat and grow. From Day 0 to Day 4, student's t-test is used, by comparing the $< BFI >_S$ between Day 0 and each day to analyze the BFI change in early incubation stage. The results of statistical analysis showed a difference of at least $P < 0.05$. The increased

development of embryo vessels and organs in the second and third quarter of the incubation period increased the $< BFI >_S$ further, as the $< BFI >_S$ and the amount of blood in the vessel are linear relationship. In the final quarter, since feathers begin to cover up the body, and the yolk sac is absorbed into the abdomen, the reflected light intensity measured from the detection fibers decreases. It shows the decreased BFI from Day 15 to Day 17. Then, the increase of $< BFI >_S$ can be explained that the movement of embryos become larger to pip internal membrane.

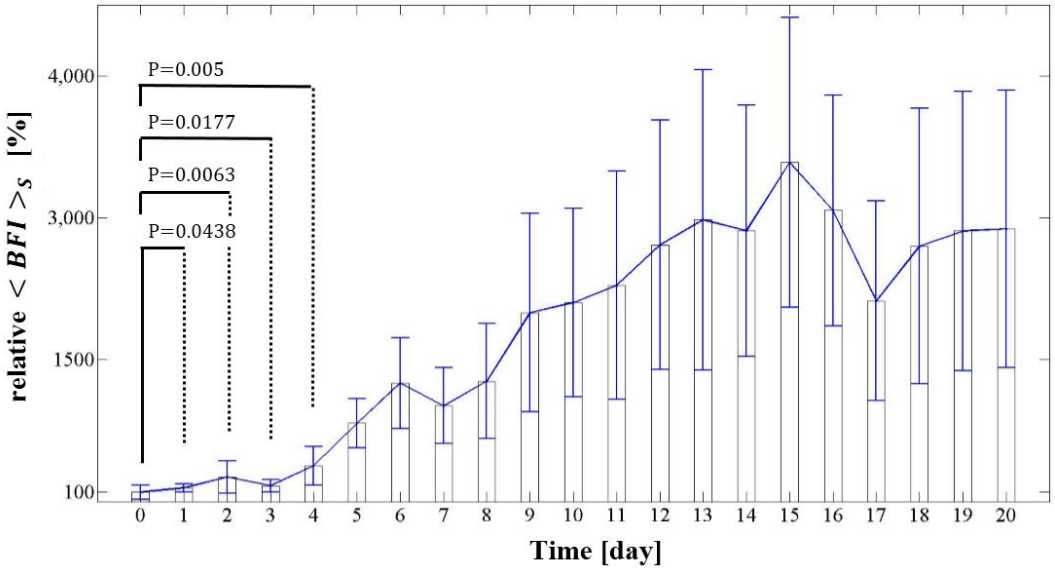

Figure 40. Change in the BFI ($< BFI >_S$) during the incubation period.

Figure 41 shows the BFI difference on the measurement positions during whole incubation periods. Because of the difference in embryo's morphology and posture, three measurement positions (M1, M2, and M3) could not distinguish each other. Therefore, the average from M1 to M3 was computed as MA. M4 is the position that the volume of the albumen is relatively larger than the yolk [7]. The BFI on the MA was higher than that of M4, as the blood volume in the embryo and yolk sac are greater.

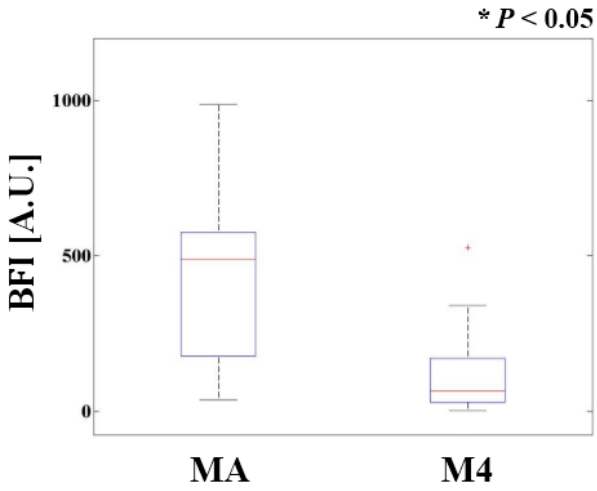

Figure 41. Mean BFIs on the all measurement positions.

To demonstrate the detectability of chick embryo vital signs, the $< BFI >_S$ from average of all measurement positions (M1 to M4) on healthy embryos was compared to the $< BFI >_S$ of weakened embryos on ten days of incubation, as shown in Fig. 42. The initial BFI represents to a healthy condition, before being delivered into a refrigerator. After 60 min, the $< BFI >_S$ relatively decreased, indicating that the embryo's condition had been weakened by the cooling process. The $< BFI >_S$ after 300 min showed 5 times difference between healthy and weakened condition. This observation supports the hypothesis that most of the BFI changes during incubation is due to the increase of real blood flow, as the only difference between the two groups is mostly the blood flow, not optical scattering or absorption. This result is similar to the result of previous approaches that reported a decrease in heart rate after the cooling process [9,10]. Therefore, these results suggest that the DSCA system could be able to monitor the vital signs of avian embryos.

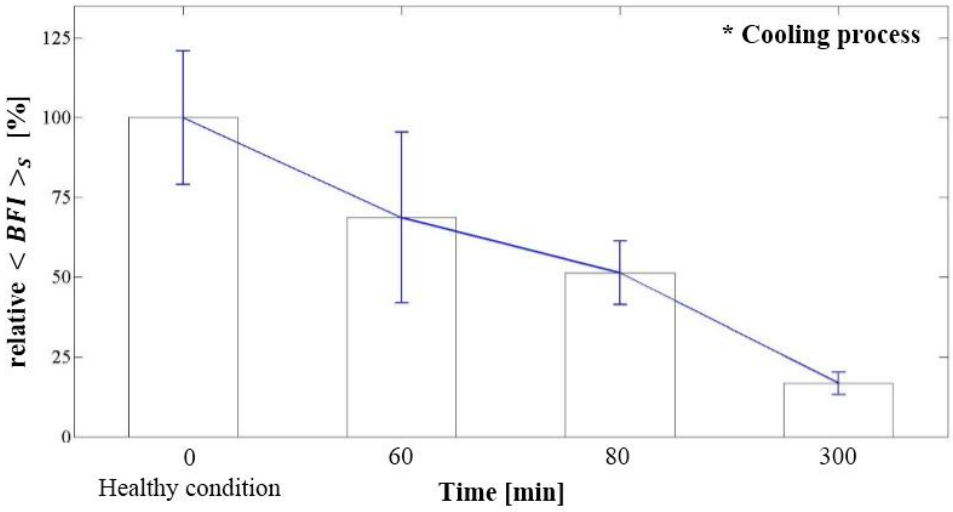

Figure 42. Change of $< BFI >_S$ during cooling process.

3.3.3 Erectile dysfunction

In third *in-vivo* application, we measured on penis during the watching sexual video to detect erectile dysfunction, as shown in Fig. 43. For the subject's private, this experiment was remotely conducted, and this experiment is applied on healthy men.

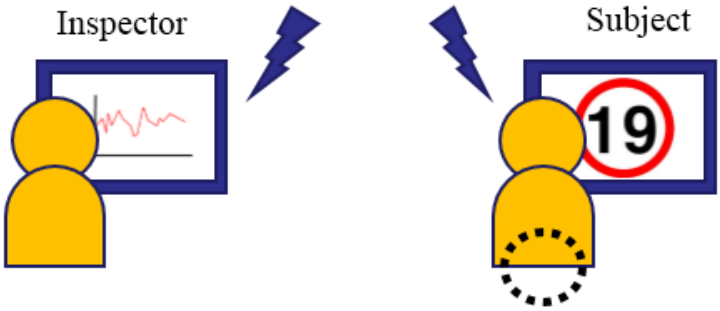

Figure 43. Schematic diagram of erectile dysfunction experiment.

Figure 44 shows schematic diagram of experimental setup. The measurement probe was attached on the top of penis to detect blood vessel. Also, we compared the sensitivity between vertical probe and horizontal probe in this experiment, as shown in Fig. 45 and 46.

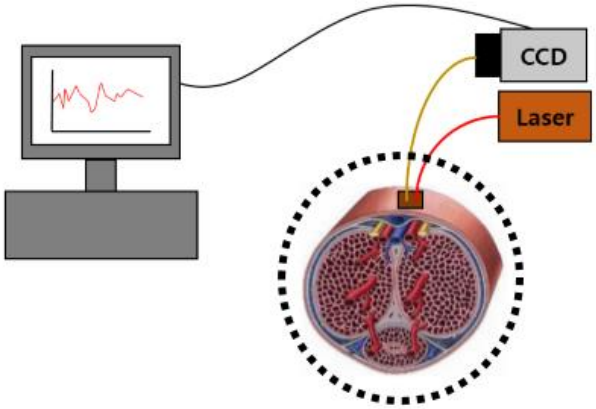

Figure 44. Schematic diagram of experimental setup in erectile dysfunction experiment.

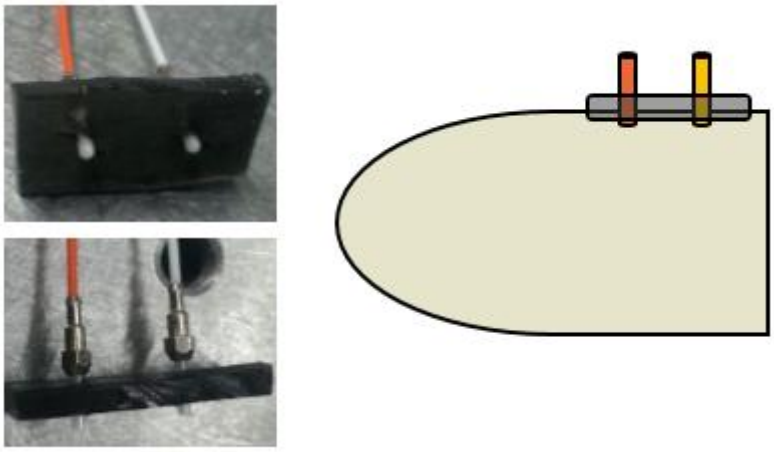

Figure 45. Vertical probe for erectile dysfunction measurement.

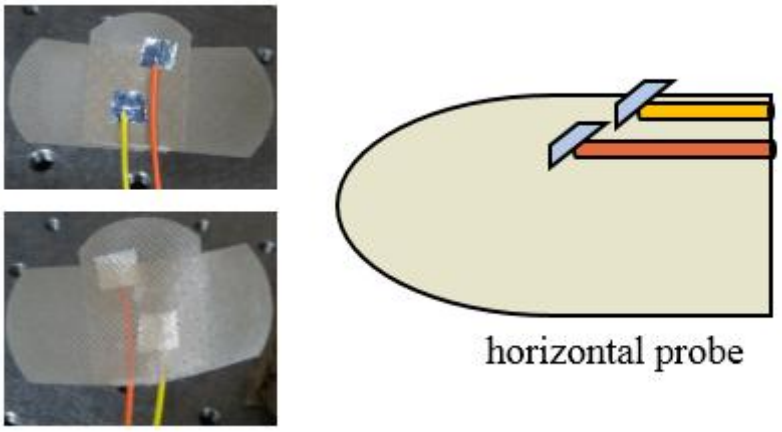

Figure 46. Horizontal probe for erectile dysfunction measurement.

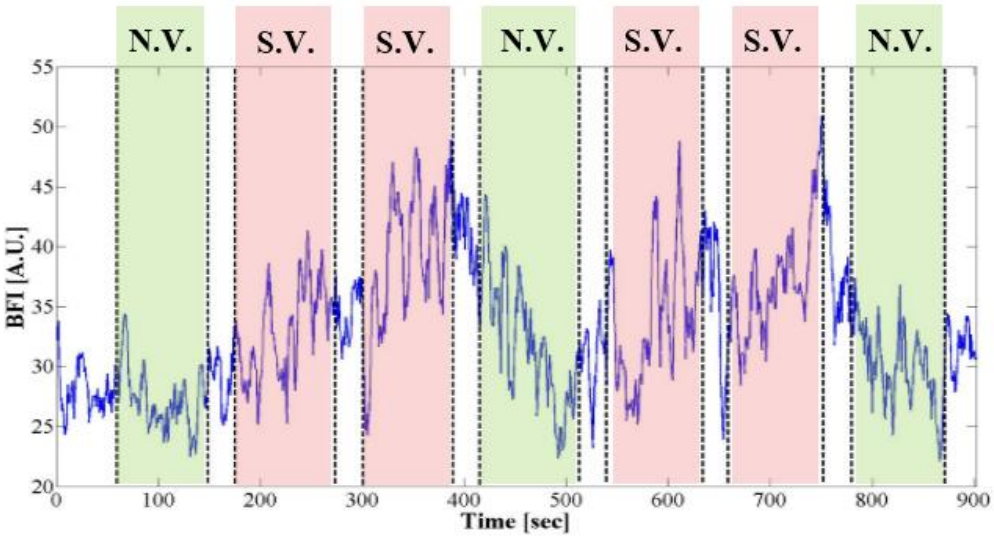

Figure 47. BFI changes of vertical probe.

Figure 47 shows result of vertical probe measurement. N.V and S.V. are natural video period and sexual video period, respectively. Other periods are rest which is no stimulation. At the first rest and natural periods, there was no significant differences of BFI. However, the BFI gradually increased at sexual video periods. Then, at the second natural video period, BFI dramatically decreased. Other periods also showed same tendency corresponding to the penile erection.

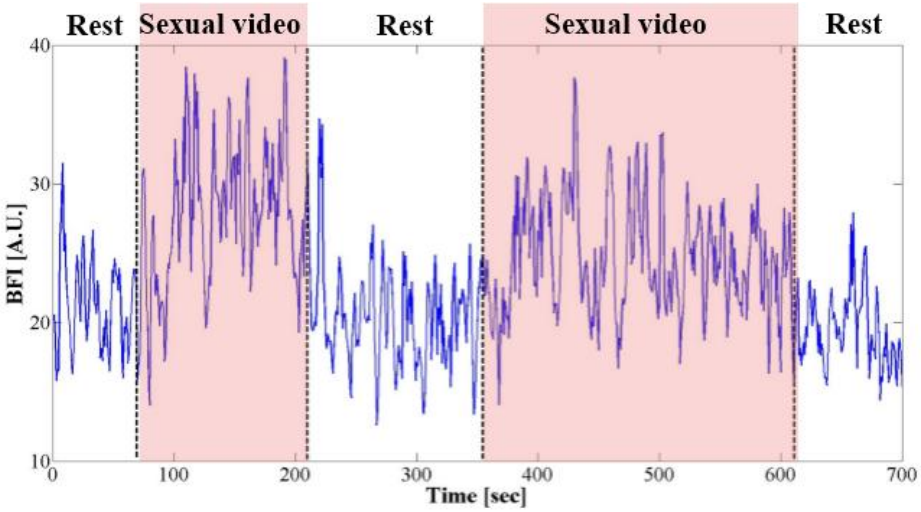

Figure 48. BFI changes of horizontal probe.

In vertical probe measurement, the BFI also changed corresponding to the different periods, as shown in Fig. 47. BFI showed result of vertical probe measurement. The BFI at the sexual video periods were larder than that of rest periods. To compare two results, the sensitivity of vertical probe experiment was better in the magnitude of the BFI change, although optical stimulation periods were different.

3.3.4 Stroke rat brain

In the experiment of stroke rat brain, there are two kinds of studies. First experiment is anesthetized rat brain monitoring, as shown in Fig. 49. The stroke rat model was induced by surgical procedures which is middle cerebral artery occlusion (MCAO). The occlusion site was left brain, and occlusion time was 90 min. In the protocol, we compared BFI between right and left brain.

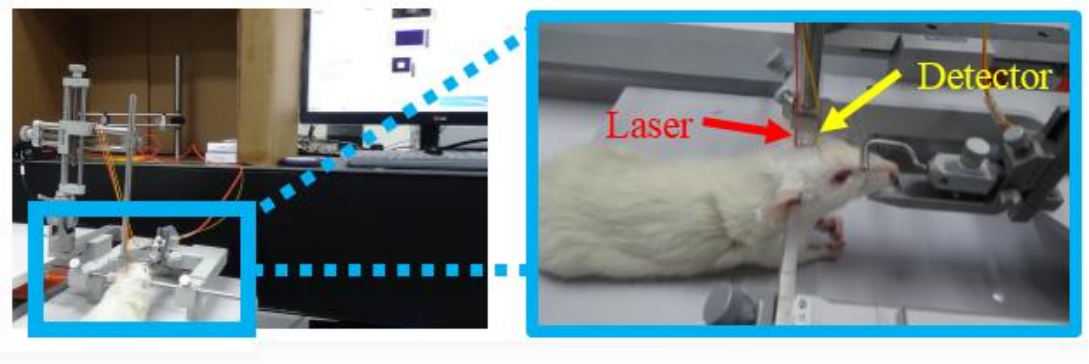

Figure 49. Experimental setup of anesthetized stroke rat brain monitoring.

As shown in Fig. 50, the BFI of left brain was lower than that of right brain corresponding to the left infarct volume. When the two BFIs were averaged, two results showed quite difference (left brain: 97.42, right brain: 125.85).

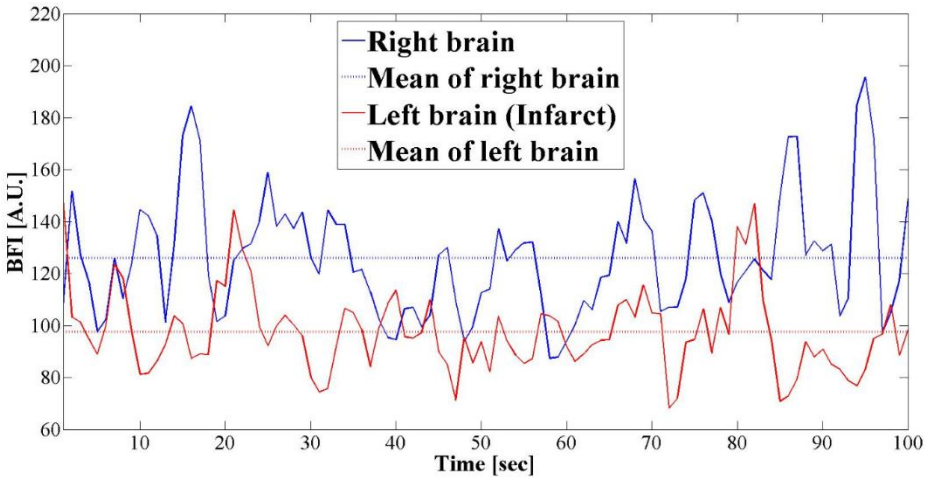

Figure 50. Experimental result of anesthetized stroke rat brain.

Second experiment is awaken stroke rat brain monitoring, as shown in Fig. 51. The rats were fixed with rat restrainer which is transparent plastic bag in order to prevent the motion artifact. To analyze brain activity after stroke rehabilitation, stroke rats were trained with a treadmill. Experimental groups were dead rat (N=1), normal rat (N=3), and training rat (N=3). The velocity of treadmill was 10 m/min. The experimental protocol of training rat group was set, as shown in Fig. 52.

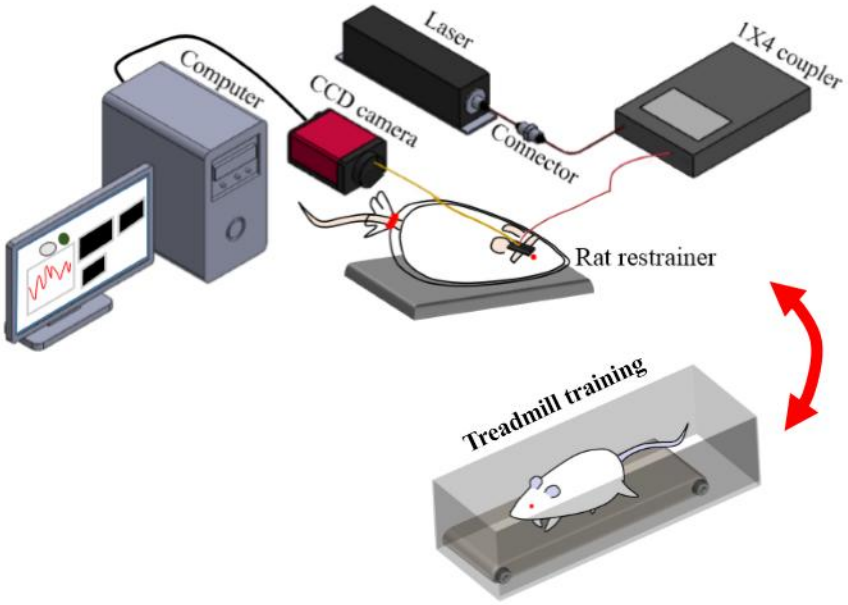

Figure 51. Experimental setup of awaken rat brain monitoring.

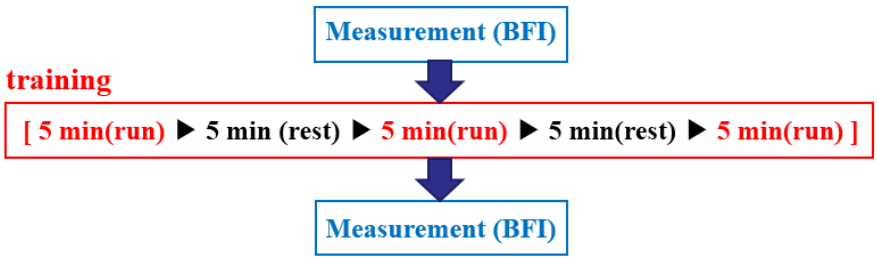

Figure 52. Experimental protocol of stroke rat brain monitoring.

Figure 53 shows the summary of experimental results of awaken rat brain. L and R in the x-axis mean left brain and right brain, respectively. The BFIs in the dead rat group showed relatively lowest among experimental groups. In the normal rat group, the distinct difference of BFIs between left brain and right brain were not shown. However, the differences were increased in stroke rat brain corresponding to the left brain infarct. The absolute changes could not be compared across the three stroke rat groups, because measurement positions were slightly changed at the every measurements. However, the difference of BFIs between left and right brain decreased in the after training group when the before and after training groups were compared.

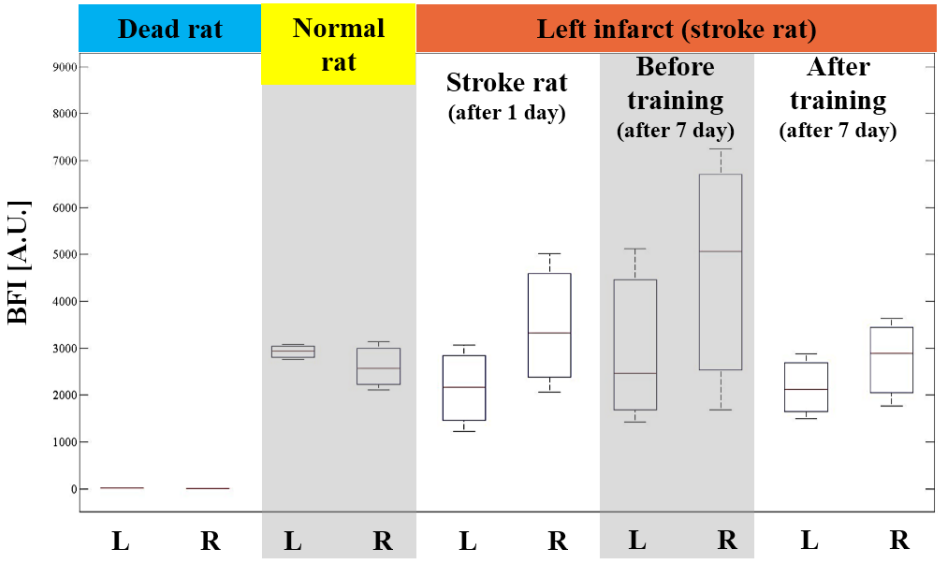

Figure 53. Experimental result of awaken rat brain monitoring.

4. Discussion and Conclusion

In this study, we designed and implemented the DSCA system. By improving the implementation of previous approaches, the DSCA system could accomplish cheaper, easier, and quantitative analysis, as well as faster image acquisition speed and the deeper flow detection. To select best type of DSCA system in the two types of data analysis, configurations, and measurement probe directions, we compared the performance of each of type in the various biological applications.

In the chick embryo experiment of mDSCA, one of the limitations is that we have used the autocorrelation function of diffuse regime throughout the incubation stages, whereas it is clear that diffuse approximation does not hold during the early incubation stage. But the egg evolves from clear to diffuse regime quite fast, and we decided to use diffuse approximation for simpler analysis. Further studies regarding accurate simulation of this transition is underway.

In the chick embryo experiment, there is a limitation that we used the autocorrelation function in diffuse regime during the incubation stages, although it is clear that diffuse approximation does not cover in the early incubation stage. To prevent biological harmful effect caused by laser power density, the laser power was adjusted to 6.9 ± 1.3 mW$/cm^2$ on the all measurement positions [10,20]; the energy was 1.38 ± 0.26 mW$/cm^2$. The egg shell was illuminated for 200 sec during each measurement cycle. While biological effects by laser illumination have been reported, no distinct difference was observed between the illuminated and non-illuminated eggs in incubated eggs.

In the early stage of embryo development, most of the volume we probe is filled with homogeneous liquid, and diffuse approximation doesn't hold in this case. Therefore, during the

early stage, the field autocorrelation function will follow the single exponential function (mostly single scattering) rather than the double exponential function (multiple scattering) that is seen as Eq. 3 in the text. As such, the speckle contrast we calculate from Eq. 2 will be also different between clear and diffuse cases. However, in the course of embryo development, the whole egg will make a smooth transition from clear to diffuse regime, and our BFI result also shows smooth and monotonous change.

The BFI that our method measures does not only depend on the scatter's movement, but also depends on changes in absorption coefficient, scattering coefficient and also the volume fraction of moving scatters to stationary scatters, as we can see from the definition of the decay factor. If the BFI were to represent true blood microcirculation, a condition has to be met such that all other factors remain stationary. As the reviewer pointed out appropriately, the chicken embryo develops organs with higher complexity as time flows, and the absorption and scattering coefficient generally increase drastically, which may contribute to the increase of BFI measurement. The point is, the BFI quantity we measured consists of contributions from all different changes that occur during embryo development, but we claim that blood flow within the embryo is the major part that causes the BFI change. And we see about 5 fold difference between living and dead. This study serves as a counterargument, as only difference between the two cases will be mostly the blood flow, not absorption or scattering.

In conclusion, we suggest the DSCA system that can monitor deep blood flow in various biological samples noninvasively. This system can distinguish the vital signs of chick embryo, erectile dysfunction, and ischemia stroke by monitoring changes of the BFI. Near future, DSCA system for blood flow monitoring would be applied in various biomedical applications. In the chick embryo, blood flow monitoring of many eggs simultaneously will be developed with automatic, accurate, and high-speed. Also, we expect that the DSCA system could become novel diagnostic and treatment monitoring system in various applications.

REFERENCES

1. T. G. Pickering, J. E. Hall, L. J. Appel, B. E. Falkner, J. Graves, M. N. Hill, D. W. Jones, T. Kurtz, S. G. Sheps, and E. J. Roccella, "Recommendations for Blood Pressure Measurement in Humans and Experimental Animals," J. Am. Heart Assoc. 111, 697-716 (2005).

2. B. Schmitz, B. W. Bottiger, and K. A. Hossmann, "Functional Activation of Cerebral Blood Flow After Cardiac Arrest in Rat," J. Cereb. Blood Flow Metab. 17(11), 1202-1209 (1997).

3. P. Vennemann, K. T. Kiger, R. Lindken, B. C. Groenendijk, S. Stekelenburg-de Vos, T. L. ten Hagen, N. T. Ursem, R. E. Poelmann, J. Westerweel, and B. P. Hierck, "In vivo micro particle image velocimetry measurements of blood-plasma in the embryonic avian heart," J. Biomech. 39(7), 1191–1200 (2006).

4. S. Rugonyi, C. Shaut, A. Liu, K. Thornburg, and R. K. Wang, "Changes in wall motion and blood flow in the outflow tract of chick embryonic hearts observed with optical coherence tomography after outflow tract banding and vitelline-vein ligation," Phys. Med. Biol. 53(18), 5077–5091 (2008).

5. M. Liu, Barbara Maurer, B. Hermann, B. Zabihian, M. G. Sandrian, A. Unterhuber, B. Baumann, E. Z. Zhang, P. C. Beard, W. J. Weninger, and W. Drexler, "Dual modality optical coherence and whole-body Photoacoustic tomography imaging of chick Embryos in multiple development stages," Biomed. Opt. Express 5(9), 3150–3159 (2014).

6. C. Andersson, J. Gripenland, and Johansson, "Using the chicken embryo to assess virulence of Listeria monocytogenes and to model other microbial infections," Nature Protocol 10(8), 1155-1164 (2015).

7. X. Li, M. Davey, S. Duce, M. Javeri, G. Liu, G. Davidson, S. Tenent, R. Mahood, P. Brown, C. Cunningham, A. Bain, K. Beattie, L. McDonald, K. Schmidt, M. Towers, C. Tickle, and S. Chudek, "Micro-magnetic resonance imaging of avian embryos," J. Anat. 211(6), 798–809 (2007).

8. L. Yang, S. You, L. Zhang, T. Yang, P. Li and Lu. J, "Noninvasive vasculature detection using laser speckle imaging in avian embryos through intact egg in early incubation stage," Biomed. Opt. Express 4(1), 32–37 (2013).

9. H. Tazawa, T. Hiraguchi, T. Asakura, H. Fujii, G. C. Whittow, "Noncontact measurements of avian embryo heart rate by means of the laser speckle: comparison with contact measurements," Med. Biol. Eng. Comput. 27(6), 580-586 (1989).

10. M. Lierz, O. Gooss, and M. Hafez, "Noninvasive heart rate measurement using a digital Egg monitor in chicken and turkey embryos," J. Avian Med. Surg. 20(3), 141-146 (2006).

11. R. Bi, J. Dong, and K. Lee, “Deep tissue flowmetry based on diffuse speckle contrast analysis,” Opt. Lett. 38(9), 1401-1403 (2013).

12. R. Bi, J. Dong, and K. Lee, and P. M. Grant, “Multi-channel deep tissue flowmetry based on temporal diffuse speckle contrast analysis,” Opt. Express 21(19), 570–578 (2013).

13. T. Durduran, R. Choe, W. B. Baker, and A. G. Yodh, “Diffuse optics for tissue monitoring and tomography,” Rep. Prog. Phys. 73, 1–43 (2010).

14. S. A. Carp, G. P. Dai, D. A. Boas, M. A. Franceschini, and Y. R. Kim, “Validation of diffuse correlation spectroscopy measurements of rodent cerebral blood flow with simultaneous arterial spin labeling MRI; towards MRI-optical continuous cerebral metabolic monitoring,” Biomed. Opt. Express 1(2), 553-565 (2010).

15. C. Huang, J. P. Radabaugh, R. K. Aouad, Y. Lin, T. J. Gal, A. B. Patel, J. Valentino, Y. Shang, and G. Yu, “Noncontact diffuse optical assessment of blood flow changes in head and neck free tissue transfer flaps,” J. Biomed. Opt. 20(7), 075008 (2015).

16. R. Bandyopadhyay, A. S. Gitting, S. S. Suh, P. K. Dixon, and D. J. Durian, “Speckle-visibility spectroscopy: A tool to study time-varying dynamics,” Rev. Sci. Instrum. 76, 093110 (2005).

17. J. D. Briers, and S. Webster, “Laser speckle contrast analysis (LASCA): a nonscanning, full-field technique for monitoring capillary blood flow,” J. Biomed. Opt. 1(1), 174–179 (1996).

18. D. A. Boas and A. K. Dunn, “Laser speckle contrast imaging in biomedical optics,” J. Biomed. Opt. 15(1), 011109 (2010).

19. R. Brown, U. Kemp, and V. Macefield, “Increases in muscle sympathetic nerve activity, heart rate, respiration, skin blood flow during passive viewing of excise,” Front. Neurosci. 102(7), 1–6 (2013).

20. R. L. Yeager, J. A. Franzosa, D. S. Millsap, J. L. Angell-Yeager, S. S. Heise, P. Wakhungu, J. Lim, H. T. Whelan, J. T. Eells, and D. S. Henshel, “Effects of 670-nm phototherapy on development,” Photomed. Laser Surg. 23(3), 268–272 (2005).

요 약 문

확산 스펙클 대비분석 시스템을 이용한 생체 내 혈류 측정

혈류 관류 또는 미소순환은 인체 건강에 있어서 중요한 역할을 한다. 이에 따라 혈류역학을 측정하는 시스템들이 많이 개발되어 왔다. 대표적으로 Laser Doppler Flowmetry, MRI, Arterial Spin Labeling 등이 있다. 하지만 개발된 장비들은 고가이며 속도가 느리고 비효율적이다. 본 연구는 경제적이며 효율적일 뿐만 아니라 깊은 혈류를 측정할 수 있는 확산 스펙클 대비 분석기 (DSCA)를 개발하였다. DSCA 의 기기장치는 Diffuse Correlation Spectroscopy (DCS) 와 유사하지만 실험적 분석은 Laser Speckle Contrast Analysis (LSCA) 와 흡사하다. DCS 는 신호처리부분에서 하드웨어 및 소프트웨어적으로 고감도의 보드가 필요하면서 고가인 단점이 있다. LSCA 는 표면 층의 혈류를 측정함으로써 깊은 혈류를 측정하지 못한다. 하지만 본 연구에서는 위 두 가지의 장점을 이용하여 설계하였다. 우선, dry phantom 을 제작하여 유동 속도에 따른 확산 스펙클 대비를 분석하였다. 실험적 결과, 유동이 있는 확산 스펙클 대비와 유동이 없는 부분에서의 확산 스펙클 대비는 확연히 차이 남을 확인하였다. 또한 주사기펌프 통한 유동속도의 변화에 따라 스팩클 대비가 선형적으로 변화하는 양상을 보였으며, 광원과 검출기간의 거리가 증가함에 따라 더 깊은 유동을 측정 할 수 있었다. Dry phantom 을 이용한 시스템 성능평가를 끝낸 뒤, 다양한 생체 실험을 위해 팔, 닭 배아, 남성 성기, 뇌 경색 모델 쥐 뇌에 적용하였다. 팔 실험에 있어서 혈압계를 이용해 팔의 혈류공급을 막고 풀었을 때 혈류지표(blood flow index, BFI)가 혈류변화와 상응한 변화를 확인하였다. 닭 배아 혈류검출 실험에서는 인공부화기에 넣기 전부터 부화되기 까지 혈류를 측정 하였을 때, 배아가 발달함에 따라 혈류지표가 증가하는 것을 확인하였다. 남성 성기 실험은 발기부전을 검출하기 위해 실험자에게 성적인 영상을 보여 주었을 때 성기에서 혈류가 어떻게 변화하는지 확인하였다. 뇌 경색 모델 쥐 뇌 실험에 있어서는 경색부위인 좌뇌와 우뇌의 혈류를 비교하였을 때 차이를 확인하여 경색부위에서 혈류지표가 더 낮은 것을 확인하였다. 여러 검증 실험을 통해 확산 스펙클 대비 분석기가 다양한 생물학적 환경에 따라 혈류역학을 분석할 수 있는 가능성을 보였으며, 본 시스템 성능이 향상된다면 각종 질환 진단에 도움을 줄 것으로 기대한다.

핵심어: 확산 스펙클 대비, 혈류지표, 유동, 혈류